ACCSCIENCE PUBLISHING

International Journal of Bioprinting

REVIEW ARTICLE

Bioprinting for organoid construction and its future application prospects

Mibo Lu[1†], Xu Chen[1†], Yalei Yin[2], Yansong Qi[3*], and Hui Xie[1*]

[1]Department of Orthopedics, Affiliated Zhongshan Hospital of Dalian University, Dalian, Liaoning, China

[2]Central Laboratory, Affiliated Zhongshan Hospital of Dalian University, Dalian, Liaoning, China

[3]Orthopedic Center (Sports Medicine Center), Inner Mongolia Autonomous Region People's Hospital, Hohhot, Inner Mongolia Autonomous Region, China

Abstract

Bioprinting technology integrates computer-aided design with precision deposition manufacturing to achieve the spatially controlled assembly of cells, biomaterials, and bioactive factors, providing important technical support for the standardized construction of functional organoids. This review systematically summarizes recent advances in bioprinting applications for organoid engineering, with particular attention to the adaptation criteria of printing technologies for different organoid systems. First, the working principles, technical features, representative commercial platforms, and application scopes of four mainstream bioprinting modalities (inkjet-based, extrusion-based, photopolymerization-based, and laser-assisted bioprinting) are summarized, and a standardized horizontal comparison of their core performance parameters is provided. Second, the classification, biological functions, and optimization strategies of three core bioink components (biomacromolecular matrices, functional cells, and bioactive factors) are comprehensively discussed. On this basis, representative research progress in seven major organoid categories, namely liver, intestinal, osteochondral, tumor, renal, cardiac, and cerebral organoids, is described, and the differential requirements of diverse organoid scenarios for printing protocols are systematically analyzed. In addition, four bottleneck challenges limiting current development are examined, including the trade-off between printing resolution and structural complexity, maintenance of cell viability and biological function, construction of hierarchical vascular networks, and cost and scalability issues, together with corresponding targeted technical solutions. Finally, future directions are discussed from the perspectives of tissue and organ regeneration, precision medicine, drug toxicity evaluation, bioink innovation, and artificial intelligence-assisted biomanufacturing (covering formulation prediction, developmental simulation, in-process quality control, and personalized structural design), aiming to provide theoretical references and technical selection guidelines for technological iteration and clinical translation in this interdisciplinary field.

Keywords: Bioprinting; Organoids; Bioinks; Tissue engineering; Regenerative medicine

[†]*These authors contributed equally to this work.*

***Corresponding authors:**
Hui Xie
(xiehui2020@163.com);
Yansong Qi
(malaqinfu@126.com)

Citation: Lu M, Chen X, Yin Y, Qi Y, Xie H. Bioprinting for organoid construction and its future application prospects. *Int J Bioprint*. 2026;12(4):026210209.
doi: 10.36922/IJB026210209

Received: May 24, 2026

1st revised: June 23, 2026

2nd revised: July 5, 2026

Accepted: July 9, 2026

Published online: July 10, 2026

1. Introduction

Three-dimensional (3D) bioprinting is an advanced interdisciplinary manufacturing

technology that integrates biomaterials science, cell biology, precision manufacturing, and computer science. At its core, it uses computer-aided design (CAD) to guide dedicated printing devices for the precise deposition of "bioinks" loaded with cells, biomaterials, and bioactive factors, enabling the fabrication of viable 3D tissues and even organ analogs. Owing to its high customizability, fine structural controllability, and cost-effectiveness in small-batch production, this technology has emerged as a core enabling platform in biomedical research and translational applications.[1] The origins of bioprinting can be traced to the 1990s, when early research primarily focused on the fabrication of acellular biomaterial scaffolds. In the early 21st century, breakthroughs in cell-printing technologies—most notably low-temperature deposition manufacturing and precision cell dispensing—drove a gradual shift in the field's research focus, moving from material-centric scaffold production to the bioprinting of functional tissue and organ constructs.[2] Key landmark developments spanning nearly four decades of advancement in this field are chronologically summarized in the timeline illustrated in Figure 1. At present, the field has developed a diversified technical system based on different material deposition mechanisms, with four mainstream modalities forming the core technical framework. Extrusion-based bioprinting drives continuous bioink filaments through pneumatic or mechanical force for layer-by-layer deposition, showing broad material compatibility and suitability for large-scale tissue construction; inkjet-based bioprinting generates uniform microdroplets through thermal, piezoelectric or acoustic pulses to achieve high-precision cell patterning; photopolymerization-based bioprinting uses light-induced crosslinking of photosensitive bioinks to fabricate constructs with micrometer-level resolution; and laser-assisted bioprinting (LAB) enables nozzle-free cell transfer through laser-induced forward transfer, reducing shear stress-induced cell damage.[3-7] In recent years, with continuous improvements in bioink formulation, printing resolution, and multicellular co-printing strategies, these technologies have overcome many limitations of traditional 3D cell culture systems and become major approaches for constructing complex 3D biological architectures. Nevertheless, important engineering bottlenecks remain to be addressed: the range of biomaterials suitable for clinical-grade bioinks is still limited, the construction of functional hierarchical vascular networks lacks mature and reliable solutions, and standardized large-scale manufacturing protocols remain insufficiently developed. These constraints have become key factors restricting further clinical translation of this technology.[8-11] Organoids are 3D *in vitro* culture models that recapitulate the structural architecture and functional phenotypes of native organs, and have become important platforms for disease mechanism research, drug screening, and regenerative medicine exploration. Conventional organoid fabrication depends largely on the spontaneous self-organization of stem cells, which inherently results in high structural heterogeneity, poor control of size and morphology, and limited tissue volume, making it difficult to accurately reproduce the spatial cellular distribution and specialized microenvironmental characteristics of *in vivo* tissues. By contrast, bioprinting allows precise regulation of organoid size, morphology, and internal microenvironment through digital modeling and precision deposition. It supports the ordered assembly of multiple cell types, biomaterials, and bioactive factors in predefined spatial patterns, thereby more closely reproducing the physiological architecture of native tissues and promoting the functional maturation of organoids.[12,13] Furthermore, standardized fabrication workflows and controllable structural and functional properties provide bioprinted organoids with better compatibility with clinical quality requirements, showing broad application prospects in personalized medicine, regenerative medicine, multi-organ model construction, and disease progression simulation.[14-18] Existing reviews in this field generally focus separately on bioprinting technology systems or organoid construction methodologies. Few studies have closely integrated these two fields to systematically clarify the selection criteria and adaptation rules of printing technologies for different organoid systems, and forward-looking analysis of emerging interdisciplinary directions such as artificial intelligence (AI)-assisted intelligent biomanufacturing remains insufficient. To address this gap, this review systematically summarizes the latest research progress of bioprinting technology in the field of organoid construction. First, it elaborates the working principles, technical characteristics, and representative commercial equipment of four mainstream bioprinting technologies, and provides a standardized horizontal comparison of core performance parameters. Second, it comprehensively discusses the classification, biological functions, and optimization strategies of the three core components of bioinks: biomacromolecular matrices, functional cells, and bioactive factors. On this basis, it summarizes representative applications and recent achievements of this technology in the construction of liver, intestinal, osteochondral, tumor, renal, cerebral, and cardiac organoids, and analyzes the matching characteristics of different printing technologies for various organoid scenarios (Figure 2). Finally, it outlines the key challenges restricting the development of this field and corresponding technical solutions, and discusses future development directions from the perspectives of tissue regeneration, precision medicine, drug toxicology

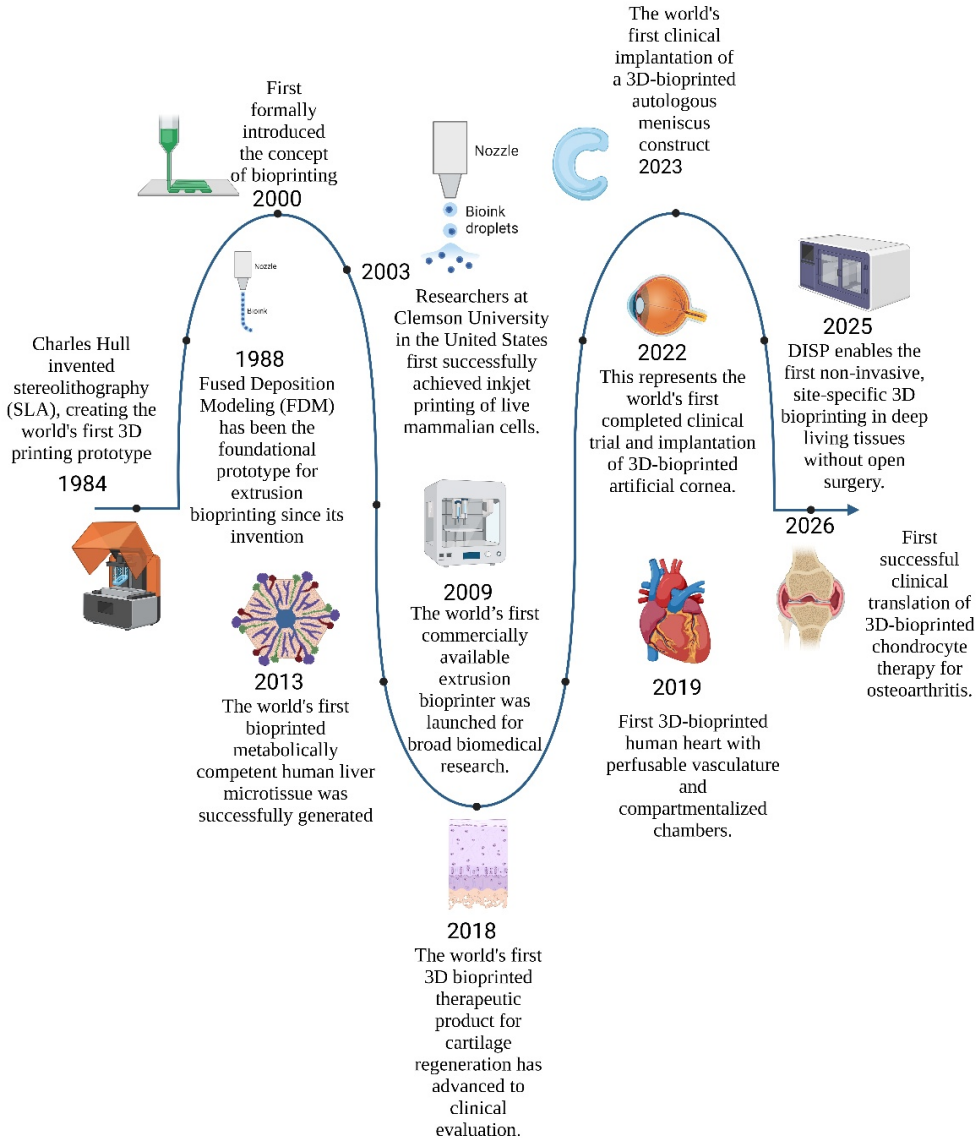

Figure 1. Timeline of the development of bioprinting technology
Abbreviation: DISP: Deep-tissue *in vivo* sound printing.

evaluation, bioink innovation, and AI-assisted intelligent biomanufacturing, aiming to provide theoretical references for technological iteration and clinical translation in this interdisciplinary field.

2. Bioprinting technologies and equipment

2.1. Inkjet-based bioprinting

2.1.1. Working principle

Inkjet-based bioprinting traces its origins to conventional graphic inkjet printing systems and ranks among the earliest technologies adapted for cell-laden biomanufacturing applications. At its operational core, the technique exploits transient pressure pulses generated via distinct physical mechanisms to atomize cell-laden bioink into uniform ultrafine droplets ranging from 10 to 100 μm in diameter. Guided by CAD models, these droplets are deposited with high spatial precision at predefined positions on a collector substrate, supporting the layer-by-layer assembly of 3D constructs. Depending on the physical principle used to generate these pressure pulses, inkjet bioprinting falls into three primary subtypes. Thermal inkjet bioprinting,

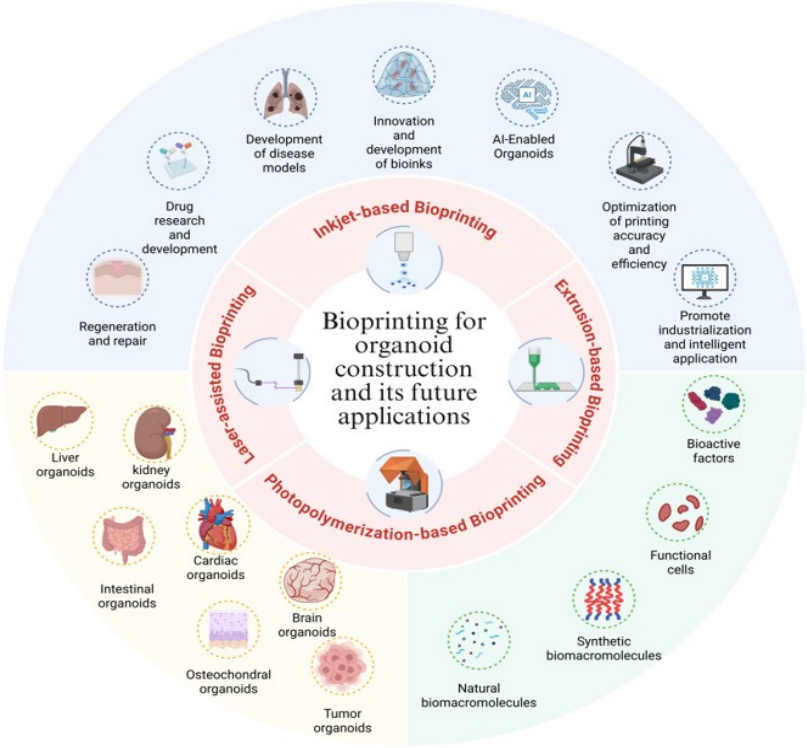

Figure 2. Bioprinting for organoid construction and its future applications. This schematic summarizes four mainstream bioprinting technologies (inkjet-based, extrusion-based, photopolymerization-based, and laser-assisted bioprinting). Centered on organoid construction, it covers core biomaterial systems, seven representative organoid types, and core applications, including regenerative repair, drug development, and disease modeling, and presents emerging directions such as bioink innovation, artificial intelligence empowerment, process optimization, and industrial implementation.

the earliest and most widely adopted variant, uses resistive microheater elements that trigger an instantaneous local temperature spike of 200 °C–300 °C in the immediately adjacent bioink. This abrupt thermal input nucleates rapidly expanding microbubbles, which create a transient pressure surge that drives discrete bioink droplets through the nozzle orifice. Piezoelectric inkjet bioprinting leverages the electromechanical coupling effect of piezoelectric materials. Under an applied voltage, the piezoelectric elements undergo rapid mechanical deformation, generating pressure waves that propagate through the bioink reservoir and force uniform bioink droplets to eject from the nozzle. The third modality, acoustic inkjet bioprinting, employs high-frequency acoustic waves to induce localized pressure fluctuations within the bioink reservoir. These acoustic perturbations deform the liquid meniscus at the nozzle outlet, triggering the controlled formation and ejection of cell-laden microdroplets without direct mechanical or thermal contact with the bioink.

2.1.2. Technical advantages and limitations

This technique mainly relies on pressure generated by acoustic waves, piezoelectric actuators, or thermal bubbles to disperse cell-containing bioinks into ultrafine droplets, which are then deposited with high precision onto predefined positions.[19,20] The advantages of this technology are particularly evident, including rapid printing speed, relatively low operating cost, and extremely high printing resolution,[21,22] which permits highly accurate cell positioning.[23] Moreover, the system can simultaneously operate multiple nozzles to print different types of cells, biomaterials, and bioactive factors in parallel, making it highly suitable for fabricating complex tissue models.[24] However, the limitations of this technology are also substantial. Inkjet-based printing imposes strict requirements on the viscosity and concentration of bioinks.[25] Excessively low concentrations reduce cell encapsulation efficiency, whereas slightly increased concentrations can easily cause nozzle blockage. Consequently, this technology is less suitable for fabricating large-scale tissues or tissues with high cell density.

2.1.3. Representative commercial equipment

Inkjet-based bioprinting ranks among the earliest bioprinting modalities to achieve widespread commercial

translation, with its hardware evolution unfolding across three distinct developmental phases. Early-generation systems were retrofitted from industrial inkjet printing platforms, with application focused primarily on single-cell microarray patterning. As the technology matured, purpose-built bioprinters emerged to enable multi-channel parallel deposition and the layer-by-layer stacking of 3D constructs. Contemporary systems are advancing toward high-throughput, high-precision customized fabrication of organoid-on-a-chip platforms. The overarching rationale behind this iterative development has been to preserve the inherent droplet precision advantage of inkjet technology while progressively expanding cell and material compatibility, boosting printing throughput, and enhancing process robustness. Currently, commercially available inkjet bioprinting platforms exhibit well-differentiated technical positioning tailored to distinct application scenarios. The MicroFab Jetlab II system (MicroFab Technologies, United States of America [USA]) serves as a longstanding benchmark platform in the field. Employing a physically actuated droplet-on-demand jetting mechanism, it generates uniform microdroplets from low-viscosity bioinks laden with viable cells and growth factors, enabling layer-by-layer site-specific deposition along preprogrammed 3D trajectories. This system has an established track record of applications in the fabrication of fine, high-resolution tissue architectures.[26] The GeSiM Nano-Plotter™ series (GeSiM, Germany) is engineered for high-throughput screening workflows. Built on high-precision piezoelectric inkjet technology, it supports nanoliter-scale droplet deposition via multi-channel parallel printheads, allowing simultaneous printing of multiple cell types and bioactive factors. This platform is widely deployed for the scalable production of cell arrays and microscale organoid chips for drug screening applications.[27] The nScrypt 3Dn-Tabletop (nScrypt, USA) extends beyond the constraints of single-modality systems by integrating piezoelectric inkjet printheads with micro-extrusion modules to enable hybrid printing across multiple bioprinting modalities. Capable of generating picoliter-scale droplets, it combines high spatial resolution with improved multi-material compatibility, making it well suited for constructing complex microtissue models containing heterogeneous multicellular components.[28] Despite these advances, prevailing commercial inkjet bioprinting systems share several inherent limitations that constrain their broader adoption. They impose strict thresholds on bioink viscosity and cell seeding density; high-concentration formulations carry a substantial risk of nozzle clogging, which hinders the fabrication of large-volume tissue constructs. In addition, residual risks of cellular damage persist across mainstream technical routes: thermal bubble inkjet systems are associated with transient temperature spikes, while piezoelectric systems expose encapsulated cells to mechanical shock during actuation. Looking ahead, three key developmental trajectories are expected to define the next generation of inkjet bioprinting hardware. The first is the development of coordinated multi-printhead control systems to enable spatially segregated, simultaneous printing of stromal cells, functional cell populations, and bioactive factors. The second is the integration of microfluidic chip technology to create unified platforms for high-throughput fabrication of organoid arrays. The third involves optimizing printhead flow channel geometries and actuation parameters to further expand the printable viscosity window and mitigate both shear-induced and thermal cellular damage.

2.2. Extrusion-based bioprinting

2.2.1. Working principle

Extrusion-based bioprinting represents the most extensively deployed and technologically mature bioprinting modality currently available. At its functional core, the technique applies controlled dispensing forces to extrude continuous bioink filaments through a micron-scale nozzle. Guided by preprogrammed CAD models, these filaments are sequentially deposited in a layer-by-layer fashion onto a motorized build platform to fabricate volumetric 3D constructs. Depending on the actuation mechanism used to drive bioink ejection from the material reservoir, extrusion bioprinting systems fall into two primary architectural categories. Pneumatic extrusion systems function by delivering regulated compressed air to the bioink reservoir, exerting homogeneous pressure across the bulk material column. This pressure drives steady, uninterrupted bioink flow through the printing nozzle to form consistent extruded filaments. Benefiting from its comparatively uncomplicated mechanical architecture, this approach exhibits broad compatibility with bioink formulations spanning a wide viscosity spectrum. Mechanical extrusion systems are further subdivided into piston-driven and screw-driven variants, distinguished by their internal force transmission components. Piston-driven platforms achieve highly precise volumetric control over dispensed bioink by modulating the linear displacement of a piston within the reservoir barrel. By contrast, screw-driven configurations employ a rotating auger mechanism to convey material, a structural design that renders them especially suitable for processing high-viscosity bioinks and formulations with high cell loading densities.

2.2.2. Technical advantages and limitations

This technique mainly uses pneumatic pressure or mechanical force to extrude bioinks through a nozzle, followed by layer-by-layer deposition along predefined pathways.[29] Since it can conveniently process high-viscosity or highly concentrated materials, extrusion-based technology shows considerable advantages in material compatibility.[30-32] It is particularly suitable for fabricating large-scale structures such as vascular, skeletal, and soft tissue models.[33] However, extrusion-based printing generally shows relatively low precision because its minimum feature size is directly limited by the nozzle diameter. In addition, the significant shear stress generated during extrusion often causes physical damage to cells, thereby affecting their final viability and biological functions.[34,35]

2.2.3. Representative commercial equipment

Extrusion-based bioprinting currently stands as the most commercially mature and widely deployed bioprinting modality across academic and industrial settings. Its hardware evolution follows a clear trajectory of upgrading from benchtop research tools to clinically translatable manufacturing platforms. Early-generation systems existed predominantly as single-actuation prototypes capable only of basic material extrusion and shaping. Subsequent iterations evolved into multifunctional platforms integrating pneumatic, piston-driven, and screw-driven actuation modes, enabling compatibility with a far broader range of material formulations. In recent years, the field has diverged into modular, benchtop, and good manufacturing practice (GMP)-grade clinical systems, designed to cover full-spectrum demands from fundamental research to industrial-scale biomanufacturing. Today's commercial extrusion bioprinting landscape features well-defined tiered market positioning tailored to distinct use cases. The BioX and INKREDIBLE+ series from CELLINK (Sweden) represent the most prevalent models in global academic research markets. Built on foundational extrusion bioprinting principles with dual pneumatic and piston-driven extrusion modes, these systems support fabrication of diverse tissue engineering constructs. They have emerged as benchmark mid-tier research-grade bioprinters, with extensive adoption in the development of *in vitro* tissue and organ models.[33,36] The 3D-Bioplotter series from EnvisionTEC (Desktop Health, Germany) is a long-established platform for high-end translational research. Supporting all three primary actuation modes—pneumatic, piston, and screw—this system accommodates an exceptionally wide viscosity window, ranging from low-viscosity cell suspensions to high-viscosity composite scaffold materials. It offers distinct advantages in osteochondral tissue engineering and large-volume tissue scaffold fabrication, making it a leading option for clinically oriented research.[37] Positioned for the entry-level basic research market, the Allevi 2 benchtop bioprinter from Allevi (3D Systems, USA) features a modular printhead design that enables multi-material co-extrusion with precise temperature control. With a low operational barrier and broad material compatibility, this system is widely deployed across universities and research institutes for routine workflows including organoid construction and bioink formulation development.[38] Despite this market diversification, prevailing commercial extrusion bioprinting systems share several fundamental technical bottlenecks that limit their performance ceiling. The primary constraint lies in print resolution, which is directly bounded by the nozzle inner diameter; minimum feature sizes rarely fall below 100 μm, preventing accurate replication of the fine microarchitectures found in native tissues. A further challenge is sustained shear stress during extrusion, which inflicts measurable cellular damage and causes pronounced viability declines in high cell-density formulations. Additionally, positional accuracy in multi-printhead coordination remains suboptimal, leaving room for improvement in fabrication consistency for complex gradient structures. Going forward, technological advancement of extrusion bioprinting hardware will unfold across four key strategic fronts. The first centers on mainstream adoption of coaxial and microfluidic extrusion technologies, which enable single-step fabrication of core-shell architectures and stratified tissue constructs. A second priority is integration of support bath (embedded) bioprinting capabilities, a breakthrough that would relax current geometric constraints on large-volume, structurally complex constructs. Third, incorporation of closed-loop pressure control and in-line optical monitoring systems will deliver improved process robustness and greater batch-to-batch printing consistency. Finally, continued development of fully enclosed, GMP-compliant clinical-grade systems will be critical to enabling downstream clinical translation and therapeutic deployment.

2.3. Photopolymerization-based bioprinting

2.3.1. Working principle

Photopolymerization-based bioprinting operates on the basis of light-triggered crosslinking, using photosensitive bioink formulations that undergo rapid solidification upon exposure to ultraviolet or visible light irradiation.[39] By directing patterned light onto discrete regions of liquid-state bioink, the technique initiates localized polymerization reactions, enabling the layer-by-layer assembly of solid 3D constructs. Based on the light delivery mechanism used to initiate crosslinking, photopolymerization bioprinting

systems fall into two primary technical categories, each with distinct curing kinetics and fabrication characteristics. Stereolithography (SLA)—the earliest developed variant—relies on a finely focused laser beam that scans the bioink surface in a pointwise raster pattern. For each layer, the laser traces the predefined cross-sectional geometry across the liquid bioink reservoir, sequentially curing only the irradiated regions into solid two-dimensional (2D) sheets. These cured layers are then stacked vertically through precise z-axis translation of the build platform, ultimately forming the complete 3D architecture. In contrast, digital light processing (DLP) systems employ a digital micromirror device as their core light-patterning component. This device projects the full 2D cross-sectional pattern across the entire bioink surface in a single exposure event, curing the complete target layer simultaneously. Unlike the serial scanning workflow of SLA, this parallel curing strategy eliminates point-by-point processing overhead, resulting in markedly higher printing speeds and overall fabrication throughput relative to point-scanning SLA configurations.[40,41]

2.3.2. Technical advantages and limitations

Compared with other bioprinting approaches, the most notable advantage of photopolymerization-based technology is its ultrahigh micrometer-scale resolution, making it particularly suitable for fabricating microfluidic chips and tissues with highly complex vascular architectures.[39] However, this technology also faces several limitations. Both the photoinitiators and the light irradiation process itself may exert cytotoxic effects. Therefore, in practical applications, irradiation parameters must be carefully controlled, photoinitiator concentrations optimized, and safer alternative materials explored to ensure cell viability and preserve normal cellular activities.[42]

2.3.3. Representative commercial equipment

Photopolymerization-based bioprinting hardware has its roots in industrial vat photopolymerization 3D printing technologies, with an overarching evolutionary rationale centered on preserving the technology's inherent ultra-high resolution while steadily advancing biocompatibility and cellular compatibility. Early-generation systems were directly repurposed from industrial SLA/DLP platforms and limited exclusively to cell-free scaffold fabrication. Subsequent developmental phases brought targeted refinements to light source wavelengths and photoinitiator formulations, expanding compatibility to cell-laden photosensitive hydrogel systems. State-of-the-art platforms are now progressing toward visible-light-driven curing, high-precision patterning, and high-throughput fabrication of customized microtissue architectures, cementing their role as foundational technologies for organoid-on-a-chip systems and microvascular network engineering. The current commercial landscape features a diverse set of platforms, each optimized for distinct technical priorities and application scenarios. The Lumen X DLP system from CELLINK ranks among the most widely adopted photopolymerization bioprinters in the field. Operating via full-layer pattern projection to enable rapid layer-wise curing, it achieves a maximum XY resolution of 25 μm and accommodates a broad range of photosensitive hydrogel formulations including gelatin methacryloyl (GelMA) and poly(ethylene glycol) diacrylate. This platform is particularly well suited for engineering highly complex microvascular networks, microfluidic organ chips, and intricate organoid microarchitectures.[43] Engineered with an industrial-grade DLP light engine, the Asiga MAX X27 bioprinter (Asiga, Australia) delivers a native XY resolution of 27 μm. Uniquely, it supports both ultraviolet and visible light curing wavelengths, enabling pairing with low-cytotoxicity visible-light photoinitiator systems. This design preserves high printing fidelity while markedly improving post-printing cell viability, leading to widespread use in microfluidic chip fabrication and biomimetic microenvironment construction.[44] Representing the current pinnacle of commercial printing resolution, the S130 micro-SLA system from BMF Precision (China) employs projection micro-SLA technology to achieve a printing accuracy down to 2 μm. This capability enables fabrication of subcellular-scale fine structures using a variety of medical-grade photosensitive resins and biocompatible hydrogels, making it ideal for cutting-edge research applications such as ultra-fine vascular networks and biomimetic organoid microscaffolds.[45] Despite these technological strides, commercially available photopolymerization bioprinting systems share several inherent limitations that restrict their broader translational potential. Printable material options remain largely confined to photosensitive modified formulations, with notably poor compatibility with unmodified native biomaterials. Conventional UV light sources and photoinitiators also carry residual risks of cytotoxicity and genotoxicity to encapsulated cells. In high cell-density bioinks, significant light scattering effects degrade crosslinking fidelity and produce blurred structural edges. Furthermore, achieving uniform through-thickness curing in large-volume, thick tissue constructs continues to pose a substantial technical challenge. Four key developmental trajectories are expected to drive advancement in this field over the coming years. First, broader adoption of visible-light and near-infrared curing technologies will further mitigate phototoxicity and improve long-term cell survival. Second, integration of two-photon polymerization capabilities

will enable 3D nanofabrication of microstructures with nanometer-scale precision. Third, the development of light scattering compensation algorithms and dynamic grayscale masking techniques will counteract resolution loss in high cell-density printing systems. Finally, coupling layer-by-layer in-line imaging with closed-loop curing parameter adjustment will enhance structural fidelity for thick tissue fabrication workflows.

2.4. Laser-assisted bioprinting

2.4.1. Working principle

Laser-assisted bioprinting, which evolved from laser-induced forward transfer (LIFT) technology, represents a nozzle-free, non-contact bioprinting modality. This contact-free operating mode circumvents key limitations of nozzle-based printing systems—most notably nozzle clogging and shear stress-mediated cellular damage—rendering it particularly well suited for rare, sensitive cell populations and high-viscosity bioink formulations.[46] At its functional core, the technique harnesses focused pulsed laser irradiation to drive controlled, precise transfer of bioink from a donor ribbon onto a receiving substrate. Deposition follows predefined CAD trajectories, enabling layer-by-layer assembly of both 2D cell arrays and 3D biological constructs. Depending on the mechanism by which laser energy is converted into the propulsive force required for bioink transfer, LAB platforms fall into two primary technical configurations. The most prevalent and widely adopted variant is dynamic release layer (DRL)-mediated LAB. The donor ribbon in this system adopts a tri-layer architecture, comprising a transparent glass carrier slide, a nanoscale metallic laser-absorbing layer (the DRL), and an overlying film of cell-laden bioink. As focused pulsed laser radiation penetrates the transparent carrier and impinges on the metallic absorbing layer, the absorbed energy induces instantaneous localized vaporization and generates high-pressure cavitation bubbles. The rapid expansion of these bubbles produces a directional propulsive force that ejects picoliter- to nanoliter-scale bioink microdroplets onto the receiving substrate. Programmable raster scanning of the laser across the donor ribbon further enables the fabrication of high-spatial-resolution 2D and 3D constructs. The second configuration, absorber-free direct LAB, dispenses entirely with the metallic absorbing layer to eliminate the risk of residual metallic particle contamination in printed constructs. In this design, the pulsed laser beam interacts directly with the bioink matrix: endogenous molecular components within the bioink absorb incident laser energy to trigger localized vaporization and subsequent droplet ejection. While this architecture enhances overall biosafety by removing exogenous metallic components, it demands more stringent parameter calibration to mitigate photothermal damage to encapsulated cells during the transfer process.

2.4.2. Technical advantages and limitations

As a nozzle-free, non-contact technology driven by pulsed laser energy, LAB fundamentally avoids nozzle clogging and reduces shear stress-induced cell damage, with cell viability generally exceeding 90%. It demonstrates excellent compatibility with rare and environmentally sensitive cells, supports a broad range of bioink viscosities and high-cell-density hydrogel systems, and achieves micrometer-level resolution with even single-cell positioning, making it suitable for constructing high-precision cell arrays and microtissue units. However, LAB is associated with relatively high equipment cost and operational complexity, resulting in a high technical threshold. Its relatively low printing efficiency also limits its suitability for large-volume organoid fabrication and high-throughput production. Conventional metal DRL systems carry potential biocompatibility risks due to particle residues, whereas absorber-free approaches require strict parameter control to avoid photothermal cell injury. Furthermore, inadequate process standardization restricts its commercialization and clinical translation.[47]

2.4.3. Representative commercial equipment

Laser-assisted bioprinting represents the latest commercial entrant and most technically demanding modality among the four mainstream bioprinting pathways. Its hardware evolution has progressed gradually from basic research prototypes toward dedicated platforms optimized for high precision and enhanced biosafety. Early iterations consisted largely of laboratory-assembled LIFT setups focused on proof-of-principle validation and single-cell patterning. Subsequent technological maturation gave rise to standardized commercial models with refined energy-absorbing layer designs and calibrated process parameters. Contemporary LAB systems are now expanding toward multi-modality integration and four-dimensional (4D) bioprinting capabilities, with a primary focus on high-end research and clinical scenarios involving rare cell populations and high-precision tissue models. The current landscape of representative commercial platforms features distinct, differentiated technical strategies. Among commercially available LAB systems, the NGB-R™ multi-modality 4D bioprinting platform from Poietis (France) stands as the most prominent LIFT-based commercial implementation. It delivers strong performance across printing resolution, cell viability, fabrication speed, and bioink compatibility, while also supporting 4D bioprinting with spatiotemporal dynamic regulation capabilities. The system has been widely adopted for engineering delicate tissue models such as skin and cornea, as well as for

high-precision tumor organoid research.[48] By contrast, the sciFLEXARRAYER S3 from Scienion (Germany) combines laser-assisted positioning with piezoelectric nanoliter dispensing technology. This hybrid configuration enables high-throughput, high-precision deposition of cells and bioactive factors, and is primarily deployed for the fabrication of microscale organoid arrays and high-throughput drug screening chips, serving a critical role in pharmaceutical research and development.[49] From an industrial development perspective, current commercial LAB systems still face multiple interconnected bottlenecks that constrain broader market penetration and clinical translation. For one, high capital procurement and maintenance costs, paired with complex operational workflows, create steep technical barriers for end users. Additionally, limited printing throughput and molding efficiency make the technology poorly suited for large-volume organoid production or large-scale manufacturing. From a biosafety standpoint, conventional metallic DRL systems carry inherent risks of residual particle contamination, while absorber-free configurations present greater challenges in parameter control and elevated risks of photothermal cellular damage. Finally, the overall lack of process standardization further restricts commercial scalability and clinical translatability. Moving forward, the evolution of LAB equipment will center on four core developmental directions. First, the advancement of absorber-free direct laser transfer technologies will eliminate metallic residue risks and elevate overall biosafety profiles. Second, the adoption of parallel laser array architectures will drive substantial improvements in printing throughput and fabrication efficiency. Third, integration of in-line quality monitoring systems with automated process parameter optimization modules will reduce operational barriers and enhance process robustness. Finally, the establishment of standardized processing protocols and quality control frameworks will be critical to accelerating clinical translation and regulatory compliance. Across the current landscape of mainstream bioprinting technologies, the four established modalities diverge substantially in core performance attributes: spatial printing resolution, post-print cell viability, and overall fabrication throughput. Their key quantitative specifications have been independently validated and calibrated against standardized protocols across an extensive body of peer-reviewed research. Drawing on harmonized measurement frameworks consolidated from prior research, this work conducts a systematic side-by-side comparison of the four technologies across six distinct technical dimensions, with their core performance parameters and corresponding application suitability summarized in detail in Table 1.

Table 1. Comparison of core parameters and characteristics of four mainstream bioprinting technologies

Technical dimension	Inkjet-based bioprinting	Extrusion-based bioprinting	Photopolymerization-based bioprinting	Laser-assisted bioprinting	References
Typical resolution	20–100 μm	100–500 μm	2–100 μm (DLP/SLA)	10–50 μm (single droplet)	9,21,39,47,50-56
Cell viability	80%–95%	70%–90%	60%–85%	90%–98%	
Printing speed	Fast (high throughput for small structures)	Medium	Fast (whole-layer curing)	Slow (low throughput)	
Bioink viscosity range	Low (1–10 mPa·s)	Wide (30 mPa·s–10^6 mPa·s)	Medium (5–300 mPa·s, photosensitive only)	Wide (1–300+ mPa·s)	
Core advantage	(i) High cell positioning accuracy (ii) Fast printing speed	Wide material compatibility, large structure fabrication	Ultrahigh resolution, complex microstructure	Ultrahigh cell viability, nozzle-free	
Core limitation	Low viscosity requirement, easy nozzle clogging	Low resolution, high shear stress	Phototoxicity risk and photoinitiator cytotoxity, limited materials	High cost, low throughput	
Representative equipment	MicroFab Jetlab II, GeSiM Nano-Plotter	CELLINK BioX, EnvisionTEC 3D-Bioplotter	CELLINK Lumen X, Asiga MAX X27	Poietis NGB-R, Scienion sciFLEXARRAYER	
Suitable organoid scenarios	High-throughput small organoid arrays, cell patterning	Large-volume organoids, osteochondral gradient structures	Microvascular organoids, organ-on-a-chip	Rare cell organoids, single-cell precision models	

3. Key components of bioinks

3.1. Biomacromolecular matrices

Biomacromolecular matrices function as the principal structural framework of bioinks. They not only determine the rheological behavior and mechanical properties of the bioink, but also provide an essential microenvironment for cellular survival and proliferation. At present, commonly used matrix materials can generally be classified into two major groups: natural biomacromolecules and synthetic polymer materials.[57]

3.1.1. Natural biomacromolecules

Since they are directly obtained from biological tissues, natural biomacromolecules possess excellent biocompatibility and cell adhesion capacity, allowing them to closely resemble the *in vivo* cellular microenvironment. Therefore, they are among the most widely used biomaterials in bioprinting applications.[58] Representative examples include collagen, alginate, hyaluronic acid, and Matrigel.

Collagen is isolated from animal tissues and represents a major component of the extracellular matrix.[59] It contains arginine–glycine–aspartic acid (RGD) sequences that promote cell adhesion [60,61] and is frequently used in skin tissue bioprinting. However, when used alone, its mechanical properties are usually insufficient, requiring combination with additional biomaterials.[62]

Alginate is a natural polysaccharide extracted from seaweed and consists of repeating β-D-mannuronic acid and α-L-guluronic acid units.[63,64] It shows excellent gelation capability and favorable biosafety and can rapidly form crosslinked structures in the presence of calcium ions.[63] However, because alginate lacks intrinsic cell adhesion sites, it is commonly combined with other hydrogel systems in practical applications.[65]

Hyaluronic acid is a linear polysaccharide composed of D-glucuronic acid and N-acetylglucosamine repeating units and can serve as a bioink material for 3D bioprinting.[66] It exhibits excellent biodegradability and low immunogenicity.[67] However, its extremely high water solubility results in relatively poor structural stability.[68]

Matrigel, a basement membrane matrix isolated from mouse tumor tissues, is widely used in organoid culture systems. It contains multiple natural extracellular matrix components that support cell proliferation. Moreover, its thermoreversible gelation characteristics help maintain gel stability under physiological conditions.[69] Nevertheless, its limited tunability in mechanical properties and animal-derived origin restrict its broader clinical application to some extent.[70]

3.1.2. Synthetic polymer materials

Hydrogel matrix materials widely adopted for bioprinting fall into two primary categories: naturally derived biopolymers and synthetic polymers. Compared with natural biomaterials, synthetic polymers offer superior controllability over mechanical properties and degradation behavior. Representative synthetic polymers are summarized below. Polyethylene glycol is a linear water-soluble polymer synthesized via ring-opening polymerization of ethylene oxide monomers.[71] It exhibits excellent hydrophilicity and minimal immunogenicity, making it particularly suitable for photopolymerization-based bioprinting applications.[72] However, its inherent bioinertness results in relatively poor cell adhesion. Polycaprolactone (PCL) possesses excellent biocompatibility and biodegradability. A key advantage of PCL is its capacity to closely mimic the native bone matrix, which underpins its widespread application in bone scaffold fabrication.[73] Polylactic acid (PLA) is a widely used biomaterial noted for its cost-effectiveness and favorable biocompatibility, with degradation products that can be readily metabolized in the human body.[74] However, PLA has limited osteoconductivity and cell-adhesive properties and may induce local inflammatory responses. Each material category presents distinct performance tradeoffs across core functional metrics—including biocompatibility, mechanical robustness, and degradation kinetics—and their fundamental material characteristics have been systematically characterized across an extensive body of biomaterials literature. A detailed comparison of the defining properties of these mainstream matrix materials is provided in Table 2.[75]

3.2. Functional cells

Cells represent the functional foundation of bioprinted organoids, and the selection and origin of these cells directly influence the functional properties and application potential of organoids. Currently, the major sources of functional cells include mesenchymal stem cells (MSCs) and pluripotent stem cells (PSCs), both of which exhibit distinct advantages and limitations, as outlined below.

3.2.1. Mesenchymal stem cells

Mesenchymal stem cells are widely recognized as one of the most promising cell sources for 3D bioprinting. Their translational appeal stems from key biological properties: multilineage differentiation potential, low immunogenicity, ease of *in vitro* expansion, and paracrine-mediated tissue regenerative capacity, all of which render MSCs well suited for functional tissue construction and clinical translation. MSCs isolated from different tissue sources exhibit pronounced heterogeneity in biological phenotypes and functional performance, alongside distinct

Table 2. Source, advantages and disadvantages of common biomacromolecular matrix materials in bioinks

Bioink	Source	Advantages	Disadvantages	References
Collagen	Animal tissues	(i) Natural biocompatibility (ii) Excellent cell affinity (iii) Controllable biodegradability (iv) Unique capability for constructing three-dimensional structures	(i) Weak mechanical properties (ii) Excessively rapid and difficult-to-control degradation rate (iii) Immunogenicity and biosafety risks	62,76-79
Alginate	Seaweed	(i) Excellent biocompatibility with low toxicity and high safety (ii) Mild ionic crosslinking preserving bioactivity	(i) Lack of cell recognition sites (ii) Weak mechanical properties and poor stability	80-82
Hyaluronic acid	Bacteria, yeast, animals	(i) Adaptable to the *in vivo* microenvironment (ii) Supports cell proliferation and differentiation (iii) Suitable for 3D bioprinting applications	(i) Lack of stable structural support (ii) Poor cell adhesion (iii) Low printing precision	83-86
Matrigel	Animal tissues	(i) Low immunogenicity and favorable biosafety (ii) Rich in natural cell adhesion sites	(i) Limited mechanical tunability (ii) Risk of animal-derived pathogen contamination (iii) Ethical and regulatory restrictions	70,87,88
Polyethylene glycol	Synthetic polymerization	(i) Ultrahigh biocompatibility and low immunogenicity (ii) High hydrophilicity (iii) Strong chemical stability	(i) Lack of biological recognition sites (ii) Limited mechanical strength (iii) Pure polyethylene glycol is non-biodegradable and may accumulate *in vivo*	89-91
Polycaprolactone	Synthetic polymerization	(i) Excellent biocompatibility (ii) Outstanding mechanical properties (iii) Biodegradability	(i) Intrinsic biological inertness and lack of cell recognition sites (ii) Poor hydrophilicity, affecting mass transport and cell adhesion	73,92,93
Polylactic acid	Plant starch	(i) Excellent biocompatibility and low cytotoxicity (ii) Superior mechanical rigidity and strength (iii) Renewable raw materials, mature industrialization, and controllable costs	(i) Intrinsic biological inertness and poor cell adhesion (ii) Extremely poor hydrophilicity, hindering mass transport (iii) Degradation products may induce local acidification and inflammation	74,94,95

inherent advantages and application limitations. The core characteristics of the three mainstream MSC populations are summarized in Table 3.

3.2.2. Pluripotent stem cells

Pluripotent stem cells (PSCs), primarily including embryonic stem cells (ESCs) and induced pluripotent stem cells (iPSCs), represent highly promising starting cell populations for bioink development in 3D bioprinting and bioprinted organoid engineering. Owing to their robust self-renewal capacity and inherent pluripotency—enabling differentiation into nearly all somatic cell types—PSCs offer an abundant, functionally diverse cellular source for bioprinting applications across bone, cartilage, myocardium, liver, neural tissue, and various organoid systems. These strengths are especially valuable for generating complex 3D tissue constructs. Despite their promise, PSC-based bioprinting faces notable translational hurdles. Incompletely differentiated cells carry inherent tumorigenic risk, and the efficiency of directed differentiation as well as the purity of resulting cell populations remain difficult to control precisely. Additionally, *in vitro*-derived differentiated cells frequently exhibit incomplete functional maturation. PSCs further display high sensitivity to bioink composition and printing parameters, introducing extra variability to fabrication consistency. Beyond these shared drawbacks, ESCs and iPSCs differ substantially in key translational aspects. ESCs are subject to distinct ethical and regulatory restrictions, while iPSC production and quality control processes are technically complex and cost-intensive. Significant

Table 3. Comparison of mesenchymal stem cells (MSCs) from different tissue sources

Source	Advantages	Disadvantages	References
Bone marrow-derived MSCs	(i) Multilineage differentiation potential with relatively low requirements for *in vitro* manipulation (ii) Low risk of malignant transformation	(i) Invasive harvesting procedures (ii) Relatively weak proliferative capacity (iii) Declining differentiation potential with aging	96-98
Adipose-derived MSCs	(i) Minimally invasive harvesting with limited donor injury (ii) High cell yield (iii) Strong paracrine functions	(i) Donor variability leads to unstable cell quality (ii) Controversies regarding potential tumorigenic risks	99-102
Human umbilical cord-derived MSCs	(i) Superior chondrogenic potential (ii) Lower risk of hypertrophy	(i) Complex preparation procedures (ii) Small sample size (iii) Potential immune responses	103-105

discrepancies between the two cell types in tumorigenic potential and directed differentiation efficiency have also been widely reported. Overall, PSCs remain an irreplaceable cellular source for the advancement of functional tissue and organ bioprinting. Table 4 provides a detailed comparative summary of their core biological and functional properties.

3.3. Bioactive factors

Bioactive factors are the key functional constituents responsible for regulatory control within bioink systems. Through multidimensional signaling pathways, these factors regulate stemness maintenance, direct lineage-specific differentiation, and promote organoid morphogenesis and functional maturation, making

Table 4. Advantages and limitations of pluripotent stem cells for bioprinted organoid construction

Cell type	Advantages	Disadvantages	References
Embryonic stem cells	(i) Intrinsic pluripotency and stable differentiation potential (ii) Well-established cell culture and differentiation systems (iii) Great potential in organoid construction (iv) Higher maturation of terminally differentiated cells and more stable functionality of printed tissues (v) Superior genomic and epigenetic stability, reducing clinical safety risks	(i) Ethical controversies and legal/regulatory restrictions (ii) Significant technical bottlenecks in precise differentiation control (iii) Complex acquisition procedures and extremely limited sources (iv) High risk of allogeneic immune rejection, preventing personalized therapy (v) Inherent teratoma formation risks and prominent safety concerns in clinical applications	12,54,106-114
Induced pluripotent stem cells	(i) Unlimited proliferative capacity enabling large-scale standardized production (ii) Broad-spectrum differentiation potential with wide application scenarios (iii) Potential for personalized therapy, fundamentally avoiding allogeneic immune rejection (iv) Free from ethical controversies and more likely to gain regulatory approval (v) Highly amenable to genetic engineering, enabling customized bioink functionalities (vi) Superior post-printing tissue self-assembly and higher maturation, closely resembling native tissues	(i) Tumorigenicity and genomic instability (ii)Low directed differentiation efficiency and insufficient maturation of terminal cells (iii) Poor tolerance to printing processes, leading to reduced cell viability (iv) High costs, lengthy production cycles, and incomplete quality-control systems for clinical-grade preparation (v)Residual risks of immune rejection (vi) Insufficient long-term *in vivo* safety and functional stability data	115-120

them indispensable functional elements of bioinks. These substances mainly include cytokines, chemokines, growth factors, hormones, and small-molecule signaling modulators.

3.3.1. Factors related to stem cell stemness maintenance and proliferation regulation

Representative molecules include epidermal growth factor, members of the fibroblast growth factor family, the Wnt signaling pathway activator R-spondin 1, and the bone morphogenetic protein inhibitor Noggin.[121] These factors function as critical regulatory components for the *in vitro* expansion and stable maintenance of stemness phenotypes in epithelial-derived organoids, such as intestinal and hepatic organoids. Incorporating these factors into bioinks through precise loading approaches can effectively maintain stem cell survival and lineage stability after the printing process. In addition, such strategies can reduce cellular heterogeneity caused by the uneven diffusion of soluble factors in traditional organoid culture systems.

3.3.2. Factors inducing directed cell differentiation and lineage specification

Representative molecules include hepatocyte growth factor, vascular endothelial growth factor (VEGF), the transforming growth factor-β (TGF-β) superfamily, and nerve growth factor. These factors mediate the directed differentiation of PSCs or adult stem cells into tissue-specific functional cells within bioprinting systems. They also participate in regulating cellular spatial organization and the establishment of cell polarity, thereby facilitating the formation and maturation of functional structural units within organoids.[122]

3.3.3. Factors regulating angiogenesis and extracellular matrix remodeling

These factors mainly include VEGF, platelet-derived growth factor, and angiopoietins. Such molecules not only stimulate the proliferation, migration, and tubular structure formation of vascular endothelial cells within bioprinted organoids, but also participate in extracellular matrix remodeling. Consequently, they provide important support for vascular network construction and cross-regional nutrient transport in large-scale organoids, thereby overcoming the persistent challenge of ischemic necrosis in the central regions of enlarged organoids during conventional culture processes.[102]

4. Specific applications of bioprinting in organoid construction

Traditional organoid fabrication mainly depends on the self-organizing capability of stem cells, making it difficult to precisely regulate organoid size, morphology, spatial cellular distribution, and microenvironmental conditions. Consequently, conventional organoids often show inherent limitations, including pronounced structural heterogeneity, insufficient functional maturation, weak batch-to-batch reproducibility, and restricted size. In contrast, bioprinting technology, through CAD and precision deposition manufacturing, enables full-process regulation of organoid fabrication from three major aspects: structure, cellular composition, and microenvironment. This technology has demonstrated enormous application potential in the construction of multiple organoid types, including liver, intestinal, osteochondral, and tumor organoids, and has become an important driving force for advancing organoid technology from fundamental research toward clinical application.

4.1. Liver organoids

Liver organoids, because of their ability to closely reproduce the native architecture and physiological functions of human liver tissue, have become important research platforms in fields such as liver disease mechanism studies, drug hepatotoxicity evaluation, and regenerative treatment of liver failure. Therefore, they possess considerable research significance and clinical application value. Although substantial progress has been achieved in liver organoid research, conventional fabrication methods still encounter multiple limitations. Traditional liver organoids not only lack the characteristic polarized organization and functional zonation of hepatic lobules *in vivo*, but also fail to realize the precise spatial positioning and ordered arrangement of multiple cell populations, including hepatocytes, hepatic stellate cells, biliary epithelial cells, and vascular endothelial cells. These shortcomings directly lead to inadequate functional maturation, inability to maintain long-term *in vitro* culture, and difficulties in constructing large-scale liver tissues, thereby greatly restricting their broader applications.[123] Bioprinting technology offers a novel technical strategy for addressing these issues. Its most significant advantage lies in the ability to accurately reproduce the characteristic hexagonal architecture and cellular spatial distribution of hepatic lobules *in vivo*, thereby enabling the fabrication of biomimetic liver organoids with physiological polarity and functional zonation and effectively compensating for the deficiencies of traditional fabrication approaches.[124] Bioprinted liver organoids are generally constructed using co-culture systems composed of hepatocyte progenitor cells differentiated from human iPSCs, primary human hepatocytes, MSCs, and vascular endothelial cells. Through multi-nozzle co-printing strategies, various cell types can be regionally distributed with high precision,

thereby simulating the distinct cellular compositions of the portal triad and central vein regions within hepatic lobules and establishing the basis for organoid functional maturation.[125] Bioink selection is another crucial factor influencing the fabrication of bioprinted liver organoids. Among currently available materials, natural hydrogels have become the predominant choice because of their excellent biocompatibility and strong cellular affinity. Collagen, Matrigel, and alginate are presently the three most widely used natural hydrogel materials. These biomaterials effectively mimic the natural extracellular matrix microenvironment of the liver, thereby providing favorable conditions for hepatocyte adhesion, proliferation, and differentiation. Simultaneously, they facilitate the reconstruction of native liver tissue architecture, thereby supporting the maintenance and maturation of hepatocyte-specific functions.[126] In recent years, several important breakthroughs have been achieved in the application of bioprinting technology for liver organoid fabrication. Shrestha *et al.*[127] leveraged microarray-based 3D bioprinting to establish a reproducible protocol for generating human liver organoids on a pillar-plate culture platform. Live/dead viability staining confirmed that both manually pipetted and bioprinted iPSC-derived organoids retained exceptionally high cellular viability (Figure 3A). When benchmarked against the conventional Matrigel embedding method in standard 24-well plates, pillar-plate-cultured liver organoids displayed a smaller, more uniform size distribution with no prominent central necrotic cores (Figure 3B). Gene expression analyses further demonstrated that bioprinted constructs exhibited comparable or elevated expression of canonical liver-specific markers—including albumin and asialoglycoprotein receptor 1—relative to conventionally prepared controls, alongside sustained expression profiles of key drug-metabolizing enzymes. Importantly, the bioprinting workflow substantially attenuated batch-to-batch variability, validating its utility as a robust and reliable platform for drug-induced hepatotoxicity screening assays (Figure 3C).[127] Furthermore, Yan *et al.*[128] adopted layer-by-layer biopatterning to fabricate large-scale liver organoids embedded with interconnected vascular networks. *In vivo* optical imaging revealed that grafts bearing biomimetic hepatic lobule architectures sustained superior long-term cell viability post-implantation (Figure 3D–3E). Hematoxylin and eosin histological staining further verified seamless integration between bioprinted constructs and native host hepatic parenchyma, accompanied by spontaneous formation of nascent microvessels within the graft boundary (Figure 3F–3G). This fabrication strategy relies on gradient VEGF release to guide directional endothelial migration and proliferation, yielding fully perfusable interconnected microvascular lumens. Such vascularized design circumvents the pervasive central necrosis defect seen in conventional liver organoids thicker than 100 μm, an issue triggered by insufficient nutrient diffusion deep inside thick tissue models.[128] Bioprinted human liver organoids have also shown promising application prospects in animal experiments. Transplantation of bioprinted liver organoids into immunodeficient mouse models of liver failure significantly enhanced mouse survival rates and effectively restored liver function parameters, thereby providing a novel technical strategy and research direction for cell-based therapies targeting end-stage liver diseases.[129]

4.2. Intestinal organoids

Intestinal organoids can effectively reproduce intestinal epithelial barriers, crypt–villus architectures, and microbiota–host interactions, thereby showing important application potential in studies related to inflammatory bowel disease, intestinal tumors, infectious diseases, and intestinal regeneration and repair.[130] In 2009, the research group led by Hans Clevers successfully established the first intestinal organoids, marking the beginning of a new era in organoid technology.[131] However, conventional intestinal organoids generated through 3D Matrigel embedding culture generally form randomly arranged cystic spheroidal structures. These organoids cannot accurately reproduce the tubular morphology of the intestine, the polarized organization of crypt–villus architecture, or the layered epithelial-stromal architecture. In addition, they fail to effectively simulate intestinal peristalsis and the microbial microenvironment, which greatly restricts their broader applications.[132] Bioprinting technology enables the precise fabrication of intestinal organoids with biomimetic tubular architectures and layered structural features, thereby overcoming the structural deficiencies of conventional intestinal organoids. Extrusion-based bioprinting can directly fabricate tubular intestinal scaffold architectures, whereas coaxial printing technology enables layered designs containing luminal, mucosal, and muscular layers, thereby accurately reproducing the anatomical characteristics of the native intestine.[133] Li *et al.*[134] leveraged embedded 3D bioprinting to fabricate large-volume intestinal constructs featuring intricate biomimetic architectures and capillary-scale vascular networks. Scanning electron microscopy analyses revealed regular, circumferential ridged structures lining the inner lumen of the printed scaffolds, which faithfully recapitulate the plicae circulares (circular folds) of native small intestinal tissue (Figure 4A). Micropores with an average diameter of approximately 200 μm were homogeneously distributed across the entire bulk of the scaffold matrix (Figure 4B). Immunofluorescence staining

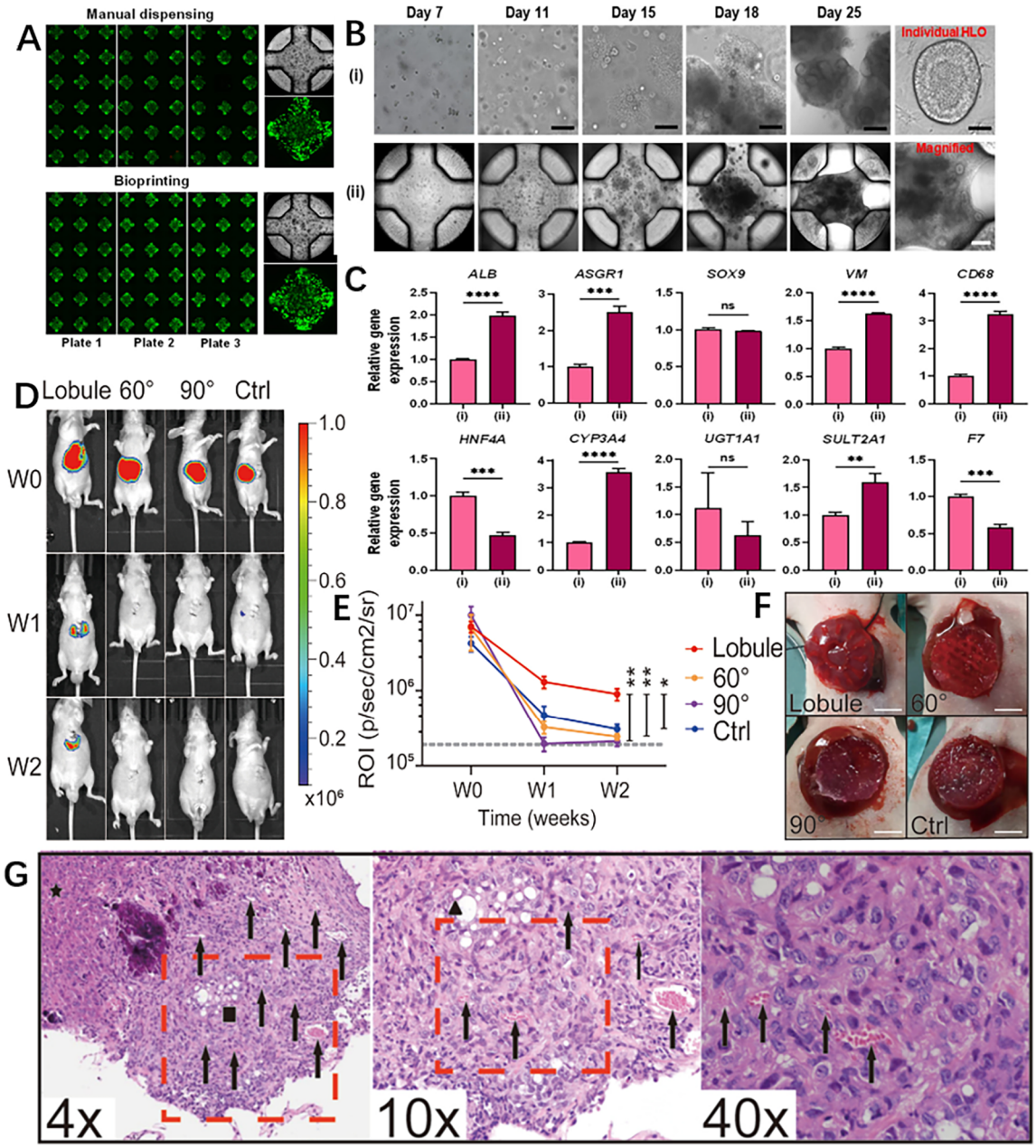

Figure 3. *In vitro* characterization of bioprinted human liver organoids and their *in vivo* engraftment with vascularized tissue integration. (A) Live/dead cell staining analysis demonstrated that both manually pipetted and bioprinted induced pluripotent stem cells maintained extremely high cellular viability. (B) (i) Human liver organoids (HLOs) cultured in 50 μL Matrigel microspheres within 24-well plates; (ii) HLOs cultured in 4 μL Matrigel spots on pillar plates. The overall morphology of organoids in both groups remained similar; however, the HLOs cultured on pillar plates were smaller, displayed improved uniformity, and showed no obvious central necrotic regions. (C) Expression levels of liver-associated biomarkers in HLOs generated in 24-well plates (i) and pillar plates (ii), including albumin (*ALB*), hepatocyte marker (*ASGR1*, *HNF4A*), cholangiocyte marker (*SOX9*), hepatic stellate cell marker (*VIM*), and Kupffer cell marker (*CD68*). Biomarker expression levels in the pillar plate group were significantly higher than or comparable to those in the 24-well plate group. The expression of genes encoding drug-metabolizing enzymes, including *CYP3A4*, *UGT1A1*, and *SULT2A1*, was comparable between the two groups, whereas coagulation factor VII (*F7*) expression was lower in the pillar-plate group. Reprinted with permission from Shrestha *et al.*[127] Copyright © 2024, Royal Society of Chemistry. (D–G) *In vivo* imaging demonstrated that the lobule-like group maintained cellular viability for the longest duration after implantation. Hematoxylin and eosin staining revealed that the grafts successfully engrafted within the host liver tissue and spontaneously formed a small number of neovessels. Magnification: 4×, 10×, and 40×. Reprinted with permission from Yan *et al.*[128] Copyright © 2025, The Authors.

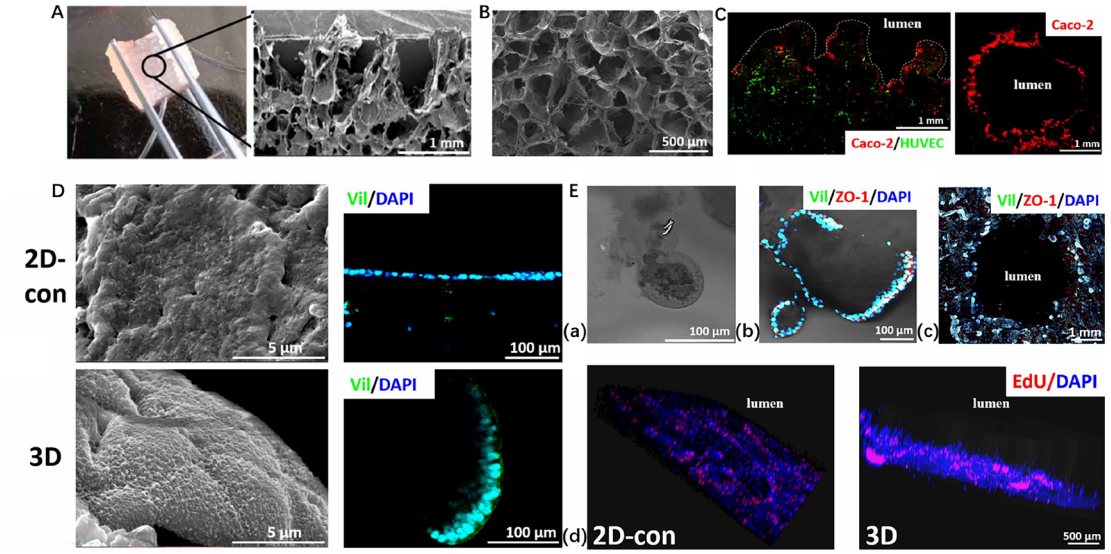

Figure 4. Structural architecture and epithelial functional maturation of large-scale biomimetic intestinal constructs fabricated via embedded 3D bioprinting. (A) Left: Photograph of the scaffold lumen showing continuous and regularly arranged circular protrusions. Right: Longitudinal cross-sectional scanning electron microscopy (SEM) image clearly illustrating regularly distributed protrusion structures that mimic the circular folds of the native small intestine. Scale bar: 1 mm. (B) SEM images demonstrating uniformly distributed micropores of about 200 μm throughout the scaffold interior. Scale bar: 500 μm. (C) Fluorescent labeling analysis: human umbilical vein endothelial cells (HUVECs) were labeled with green DiO, whereas Caco-2 cells were labeled with red DiI. The results showed that HUVECs were uniformly distributed throughout the scaffold body, while Caco-2 cells adhered to and proliferated along the luminal folds, thereby forming a layered structure closely resembling that of the native intestine, with the epithelial layer positioned above and the vascular layer beneath. Scale bar: 1 mm. (D) 2D planar model: SEM images revealed sparse and short microvilli without the formation of a continuous brush border (scale bar: 5 μm). Immunofluorescence staining for Villin, a microvillus-specific marker, showed weak and unevenly distributed fluorescence signals (scale bar: 100 μm). 3D intestinal model: SEM images demonstrated surfaces densely covered with elongated and highly organized microvilli, forming a continuous brush border structure (scale bar: 5 μm). Villin fluorescence signals were strong and uniformly distributed (scale bar: 100 μm). (E) (a–c) Observation of budding structures. After 14 days of culture, Caco-2 cells formed single-cell-layer bud-like protrusions about 100 μm in size, highly resembling the budding morphology of intestinal organoids cultured in Matrigel. Immunofluorescence analysis demonstrated high expression levels of Villin and ZO-1 within these budding structures, confirming their identity as functional epithelial architectures. Scale bar: 100 μm/1 mm. (d) EdU staining of proliferating cells. In the 2D model, proliferating cells were evenly and sparsely distributed. In contrast, proliferating cells in the 3D model clustered together and migrated inward into the scaffold interior, thereby forming crypt-like invaginated structures. Scale bar: 500 μm. Reprinted with permission from Li *et al.*[134] Copyright © 2024, IOP Publishing Ltd.

further validated that human umbilical vein endothelial cells (HUVECs) were evenly dispersed throughout the scaffold body, while Caco-2 epithelial cells adhered and proliferated selectively along the luminal folds. This spatial arrangement gave rise to a stratified tissue hierarchy with an apical epithelial layer overlying a basal vascular compartment, closely recapitulating the native layered organization of intestinal tissue (Figure 4C). Relative to conventional 2D planar culture models, the bioprinted 3D intestinal constructs developed denser, more orderly arranged surface microvilli that formed a contiguous brush border structure. The 3D constructs also displayed higher and more uniformly distributed expression of villin protein, a canonical marker of intestinal epithelial differentiation (Figure 4D). Following 14 days of *in vitro* cultivation, Caco-2 cells formed bud-shaped morphologies reminiscent of native intestinal organoid budding. Proliferative cell populations aggregated and migrated inward into the scaffold interior, giving rise to crypt-like invagination structures characteristic of native intestinal crypts (Figure 4E).[134] Existing studies have successfully used bioprinting technology to fabricate tubular intestinal organoids with functional crypt–villus topological architectures. These printed organoids can form structurally and functionally intact intestinal epithelial barriers. Transepithelial electrical resistance (TEER), a key parameter reflecting epithelial barrier integrity, was significantly higher in these bioprinted tubular organoids than in conventional cystic intestinal organoids generated through traditional culture systems. Building on prior bioprinting workflows, Torras *et al.*[135] engineered a 3D intestinal model featuring biomimetic crypt–villus topographies. Bright-field imaging confirmed uniformly distributed villus arrays across the printed constructs, while cross-sectional characterization

corroborated the full 3D crypt–villus architecture and high dimensional fidelity of the fabricated tissues (Figure 5A). Cultures supplemented with stromal fibroblasts developed markedly more mature epithelial phenotypes after 21 days of *in vitro* cultivation, relative to epithelial-only control groups (Figure 5B). Immunofluorescence staining verified the presence of intact basement membranes and cytoskeletal networks within the engineered model (Figure 5C), with quantified structural parameters closely aligning with the physiological dimensions of native human small intestine (Figure 5D). Additional labeling of extracellular matrix proteins and intercellular junction markers further corroborated both the structural integrity and functional maturity of the fabricated tissue constructs (Figure 5E–5F). Functionally, this model exhibited significantly elevated TEER compared with conventional cystic intestinal organoids, enabling robust and reproducible recapitulation of core intestinal epithelial functions including molecular transport, nutrient absorption, and barrier defense.[135] In the field of regenerative medicine, bioprinted tubular intestinal organoids have shown the ability to effectively restore intestinal function in mouse models of short bowel syndrome. Following transplantation, these organoids integrated with host intestinal tissues and formed mature epithelial structures, significantly improving nutrient absorption capacity in mice. These findings provide a promising novel strategy for the treatment of intestinal defect-associated diseases.[136]

4.3. Osteochondral organoids

The repair and regeneration of osteochondral defects caused by trauma and degenerative disorders remain major clinical challenges in the fields of orthopedics and sports medicine. Conventional therapeutic approaches, including autologous bone grafting and artificial joint prosthesis implantation, are associated with several inherent

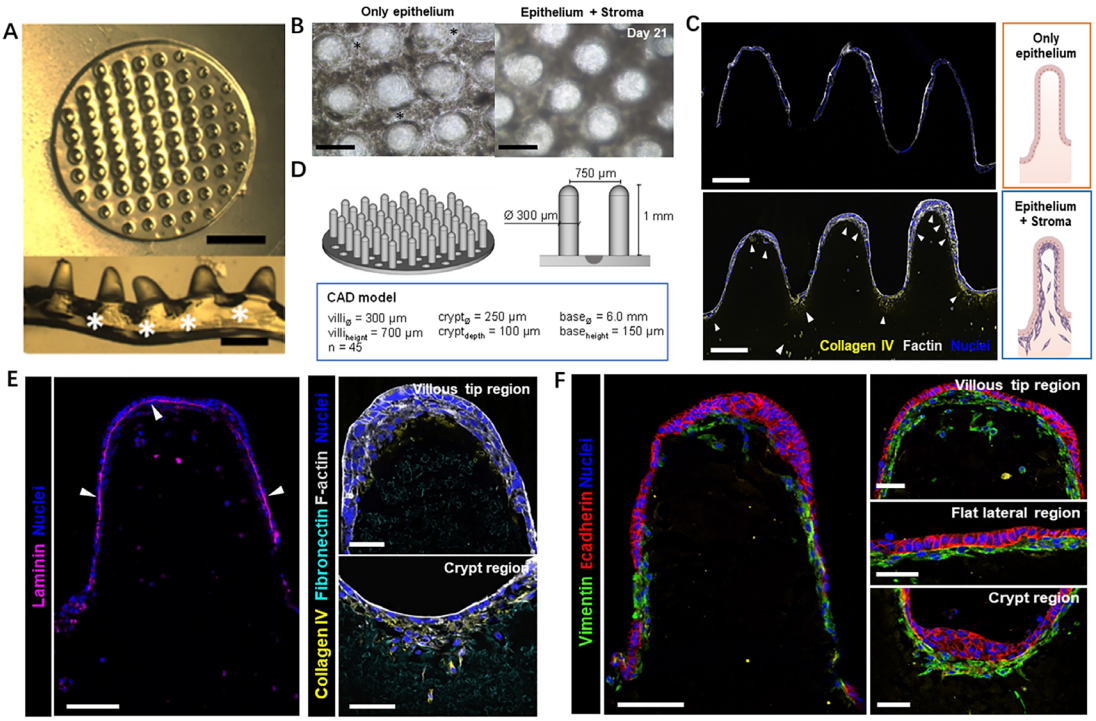

Figure 5. Structural fidelity and epithelial barrier function of a 3D-bioprinted intestinal model with biomimetic crypt–villus topography. (A) Bright-field images of the printed constructs. The top-view image (scale bar: 1.5 mm) demonstrates a uniformly distributed villus array, whereas the cross-sectional image further confirms the three-dimensional crypt–villus architecture and dimensional fidelity. Scale bar: 400 μm. (B) Bright-field images obtained after 21 days of culture (scale bar: 100 μm). Control group: blank hydrogel without stromal cells seeded with Caco-2 cells. Experimental group: NIH-3T3-containing hydrogel seeded with Caco-2 cells. Scale bar: 100 μm. (C) Immunofluorescence staining of tissue sections. F-actin (gray) indicates the cytoskeleton, type IV collagen (yellow) labels the basement membrane, and DAPI (blue) stains cell nuclei. Scale bar: 200 μm. (D) Structural parameters: base diameter of 6.0 mm and thickness of 250 μm; villus height of 700 μm and diameter of 300 μm; crypt depth of 150 μm and diameter of 250 μm, fully corresponding to the physiological dimensions of the human small intestine. (E) Extracellular matrix protein staining: laminin (magenta), type IV collagen (yellow), and fibronectin (cyan). Scale bar: 100 μm. (F) Cell-type and junction marker staining (scale bar: 100 μm): E-cadherin (red) marks epithelial cell junctions, while vimentin (green) marks stromal fibroblasts. Scale bar: 100 μm. Reprinted with permission from Torras *et al.*[135]

shortcomings, such as secondary donor-site injury, inadequate tissue compatibility, long-term prosthesis loosening, and limited implant durability.[137] At present, osteochondral organoids fabricated using traditional construction systems still face major technical barriers. These systems cannot accurately reproduce the spatial gradient architecture and gradient mechanical characteristics of native osteochondral tissues, nor can they achieve the ordered reconstruction of the triphasic hierarchical structure composed of the hyaline cartilage layer, calcified cartilage layer, and subchondral bone. In particular, the characteristic arcade-like collagen network of articular cartilage, which plays a crucial role in tissue mechanical strength and load-bearing capacity, is extremely difficult to precisely reconstruct using conventional approaches. As a result, engineered cartilage shows mechanical performance far inferior to that of native tissue and demonstrates poor long-term stability *in vivo*. Moreover, the overall mechanical strength of conventional organoids is insufficient to withstand the physiological mechanical environment of load-bearing regions, thereby greatly limiting their translational application potential for *in vivo* tissue repair.[138] As a digital additive manufacturing strategy, 3D bioprinting enables precise spatial positioning and controllable deposition of biomaterials and functional cells, thereby allowing highly accurate customization of the multiscale architecture and mechanical properties of engineered constructs. Consequently, it has become a central technological platform for fabricating biomimetic hierarchical osteochondral organoids. Its unique advantage lies in its ability to realize integrated biomimetic design and fabrication of gradient structures, heterogeneous cellular compositions, and gradient mechanical properties of osteochondral composite tissues within a single fabrication process, thereby closely matching the physiological architecture and functional features of native osteochondral tissues. At the material-system design level, 3D bioprinting of osteochondral organoids commonly uses soft–stiff gradient composite bioink systems. Natural polymer-based hydrogels are generally selected for fabricating the cartilage layer because these materials possess biocompatibility and network structures similar to the extracellular matrix of native cartilage, thereby enabling accurate matching of the low-modulus, high-resilience mechanical properties and physiological microenvironment of hyaline cartilage tissue. In contrast, the subchondral bone layer is usually fabricated using biodegradable aliphatic polyesters such as PCL and PLA, combined with calcium phosphate bioceramics, including hydroxyapatite, to form composite systems. These materials markedly improve the mechanical strength and structural stability of printed scaffolds while simultaneously mimicking the rigid support function and osteogenic microenvironment of subchondral bone tissue. Ultimately, multicomponent gradient printing strategies enable continuous transitions in mechanical properties from the cartilage layer to the subchondral bone layer, thereby reproducing the natural mechanical gradient characteristics of the osteochondral interface.[139] To address insufficient endogenous stem cell recruitment, limited vascularization, and inadequate osteoinductive activity in acellular bone repair scaffolds, Cao et al.[140] incorporated 10% injectable platelet-rich fibrin (i-PRF) and 1% synthetic magnesium silicate nanoclay (Laponite [Lap]) into an alginate methacryloyl/GelMA–methylcellulose (abbreviated AGM) bioink and fabricated porous i-PRF-AGM@Lap hydrogel scaffolds using 3D bioprinting. Transwell migration assays revealed a synergistic chemotactic effect between growth factors released from i-PRF and Mg^{2+}/Si^{4+} ions eluted from Lap, which drove maximal directional chemotactic migration of bone marrow-derived mesenchymal stem cells (BMSCs) (Figure 6A–6C). Wound scratch assays corroborated these pro-migratory effects, demonstrating that the optimized composite scaffold markedly enhanced BMSC motility and *in vitro* wound closure efficiency (Figure 6D–6E). CD44/F-actin immunofluorescence staining further validated the superior recruitment performance of this formulation: adherent BMSCs exhibited a canonical spindle-shaped morphology and achieved the largest cell spreading area among all experimental groups (Figure 6F).[140] In recent years, articular cartilage progenitor cells (ACPs), as a novel cartilage-specific seed cell type, have demonstrated significantly greater chondrogenic potential than mature chondrocytes and MSCs. In 2026, Karam *et al.*[141] demonstrated that ACPs isolated from the superficial zone of goat articular cartilage through differential fibronectin adhesion methods exhibited characteristic spindle-shaped morphology and markedly enhanced chondrogenic differentiation capability compared with donor-matched mature chondrocytes. During a three-week pellet culture period, ACPs secreted 1.5-fold higher levels of sulfated glycosaminoglycans and twofold greater total collagen content than mature chondrocytes, while also showing stronger type II collagen staining. Importantly, no type X collagen expression or calcium deposition was detected throughout the culture process. ACPs could therefore stably preserve the hyaline cartilage phenotype while avoiding the hypertrophic calcification commonly observed in MSCs, suggesting that these cells may represent an ideal cellular source for constructing functional cartilage organoids.[141] A key strategy for cellular system construction involves region-specific functional modification of bioinks. Specifically, different regions corresponding to the cartilage

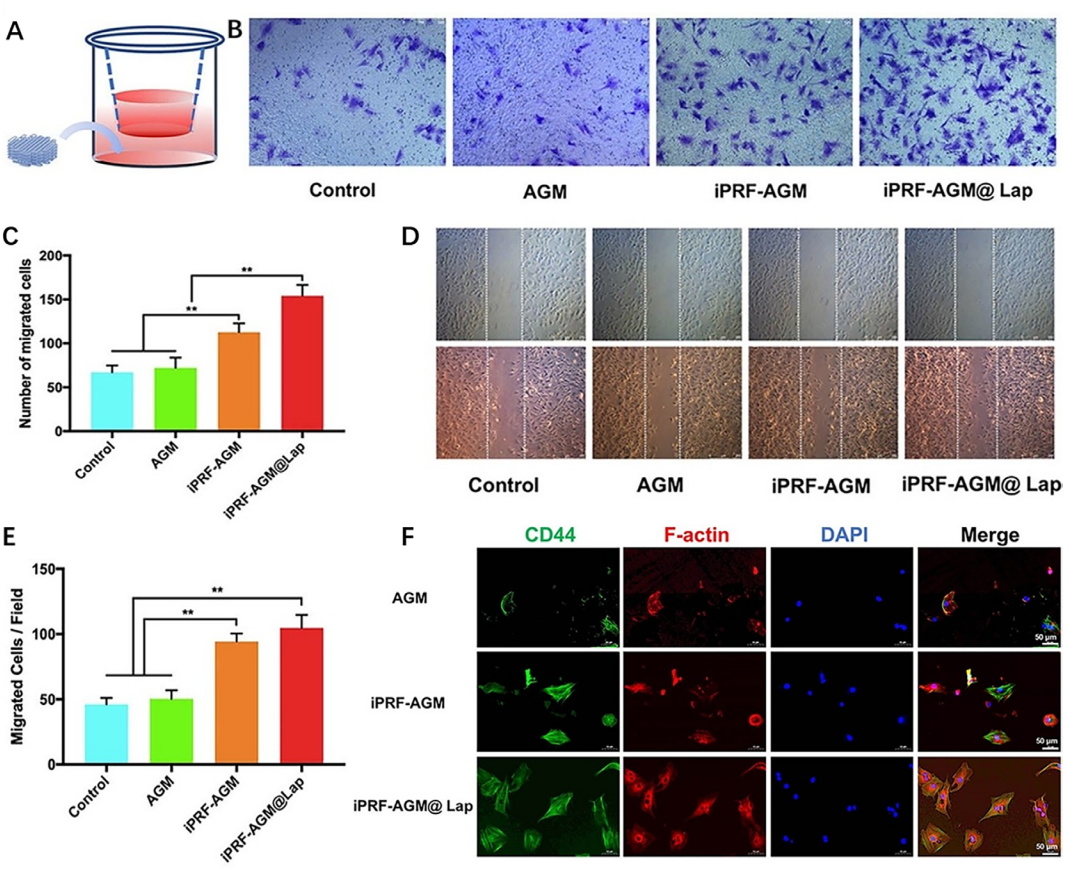

Figure 6. Synergistic chemotactic recruitment of BMSCs by i-PRF and Lap-reinforced composite bioinks. (A) Schematic diagram illustrating the *in vitro* directional recruitment and chemotaxis experiment of BMSCs. (B) Transwell cell migration assay. The i-PRF-AGM@Lap group was identified as the optimal experimental condition. Growth factors released from i-PRF together with bioactive ions (Mg^{2+} and Si^{4+}) derived from Lap exhibited synergistic recruitment effects, and their combined action maximally promoted the directed chemotaxis and migration of BMSCs. (C) The y-axis represents the number of BMSCs migrating through the porous Transwell membrane, whereas the x-axis indicates the experimental groups. The i-PRF-AGM@Lap group demonstrated the highest level of BMSC migration. (D) Scratch wound-healing assay. In the i-PRF-AGM group, growth factors released from i-PRF within the scaffold, including vascular endothelial growth factor, platelet-derived growth factor, and transforming growth factor-β, significantly enhanced BMSC migration, crawling, and wound closure, indicating that these growth factors function as the principal active components driving stem cell migration. In the optimized i-PRF-AGM@Lap composite group, synergistic interactions between i-PRF-derived growth factors and Lap-derived bioactive ions (Mg^{2+} and Si^{4+}) maximally enhanced BMSC migration, crawling behavior, and wound-healing capability. (E) The y-axis represents the number of BMSCs migrating into the scratched blank region within each microscopic field, while the x-axis represents the experimental groups. The i-PRF-AGM@Lap group exhibited significantly higher numbers of migrated cells than the i-PRF-AGM group, reaching peak migration levels. (F) CD44/F-actin immunofluorescence staining demonstrated that the i-PRF-AGM@Lap group exhibited the strongest BMSC recruitment capability. The adherent cells displayed a typical spindle-shaped morphology and the largest spreading area. Scale bar: 50 μm. Reprinted with permission from Cao *et al.*[140] Abbreviations: AGM: Alginate methacryloyl/GelMA–methylcellulose; BMSCs: Bone marrow mesenchymal stem cells; i-PRF: Platelet-rich fibrin; Lap: Laponite.

and bone layers of native osteochondral tissues are loaded with lineage-specific inductive cytokines within the same printed construct. The cartilage region is enriched with chondrogenic differentiation-inducing factors represented by TGF-β3, whereas the bone region contains osteogenic differentiation-inducing factors centered on bone morphogenetic protein-2. This strategy enables spatially controlled lineage-specific differentiation of MSCs within a single printing platform, thereby accurately reproducing the hierarchical spatial distribution pattern of native osteochondral tissues *in vitro*.[142] In *in vivo* animal studies conducted by Chen *et al.*[143], chondrogenic organoids differentiated from BMSCs were blended with GelMA hydrogel and implanted into surgically created osteochondral defects. Gross morphological observation revealed full defect regeneration in groups receiving organoid-laden GelMA constructs. The regenerated tissue formed smooth superficial cartilage that fused seamlessly

with adjacent native cartilage, accompanied by abundant, uniformly thickened trabecular bone exhibiting robust integration with host osseous tissue (Figure 7A). Quantitative metrics including International Cartilage Repair Society (ICRS) scores, trabecular thickness, and bone volume fraction all reached markedly elevated levels relative to blank control cohorts (Figure 7B). Histological staining further confirmed complete recapitulation of tri-layered osteochondral architecture within treatment groups, consisting of superficial cartilage, intermediate transitional zones, and subchondral bone, with tight bonding to peripheral host tissue (Figure 7C).[143] At present, 3D bioprinting technology has been successfully applied for the fabrication of integrated osteochondral organoids with layered architectures. During long-term *in vitro* culture, these organoids can achieve synchronized maturation of both cartilage and bone layers. Complementary *in vitro* co-culture assays further demonstrated that stratified scaffolds seeded with dense cell populations could boost extracellular matrix deposition within osteochondral co-culture systems. Enzyme-linked immunosorbent assay quantification illustrated elevated secretion of collagen type I and aggrecan in co-culture batches compared with single-cell-type monocultures; samples loaded at higher cell densities yielded even greater production of these matrix biomolecules (Figure 7D). These quantitative readouts substantiate that graded cell density layouts exert stimulatory effects on synchronized maturation of engineered osteochondral organoids.[144] In the future, combining pure-cell bioprinting with physical boundary regulation strategies may enable the fabrication of fully biomimetic osteochondral organoids possessing both osteochondral interfacial gradients and the internal collagen arcade architecture of cartilage, thereby substantially improving their *in vivo* repair efficacy and long-term stability.

4.4. Tumor organoids

Tumor organoids can accurately recapitulate the genomic features, intratumoral heterogeneity, and clinically relevant drug-response phenotypes of primary tumors, making them a central platform in precision oncology research. They have shown irreplaceable value in several important research fields, including tumor pathogenesis analysis, personalized anticancer drug screening, and *in vitro* modeling of the tumor immune microenvironment.[145] The integration of bioprinting technology further enables the precise and controllable fabrication of tumor organoids with spatial heterogeneity and highly biomimetic tumor microenvironments. The major advantage of this technology lies in its ability to precisely regulate the spatial distribution of tumor cells, stromal cells, immune cells, and vascular endothelial cells, thereby reconstructing the pathological architecture, stromal mechanical stiffness, and nutrient gradients of tumor tissues *in vitro*. Thus, it allows accurate simulation of the complete biological processes involved in local tumor invasion and distant metastasis.[146] In bioprinted tumor organoid systems, the core cellular strategy is based on multicellular co-culture models. These systems usually include patient-derived cancer cells, cancer-associated fibroblasts, tumor-associated macrophages, vascular endothelial cells, and various functional immune cells. Such co-culture systems can closely reproduce the cellular heterogeneity of primary tumors in a 3D *in vitro* environment while reconstructing the composition and functional features of the tumor immune microenvironment. Among these components, patient-derived cancer cells serve as the central functional component of the co-culture system, maintaining the genomic mutation patterns and clinical drug-response phenotypes of primary tumor tissues. Therefore, bioprinted tumor organoids constructed using these multicellular systems provide highly reliable *in vitro* models for personalized anticancer drug screening in clinical oncology patients (Figure 8D).[106] In the 3D bioprinting of tumor organoids, bioinks serve as the core matrices for cell support and microenvironment construction, and the selection and regulation of bioink materials directly influence organoid fabrication outcomes. For example, hepatocellular carcinoma tissues are characterized by loose stromal organization and naturally low mechanical stiffness; therefore, liver tumor organoids are generally printed using low-stiffness Matrigel-collagen composite hydrogels. By contrast, pancreatic cancer is characterized by dense stromal tissues and high mechanical stiffness, and its organoid printing systems commonly use high-stiffness fibrin-hyaluronic acid composite hydrogels to better mimic the native tumor microenvironment.[107] Compared with conventional 2D cell culture systems, 3D-bioprinted glioma organoids show drug-resistance phenotypes that more closely resemble those of clinical primary tumors. Their resistance profiles are therefore more clinically relevant, allowing them to function as physiologically relevant and predictive *in vitro* models for anticancer drug screening and therapeutic efficacy prediction.[54] Moreover, research groups have used multimaterial layered bioprinting technologies to fabricate biomimetic tumor organoids containing 3D tumor-stroma-vascular interfaces. These *in vitro* models can accurately reproduce the pathophysiological processes of tumor angiogenesis and distant metastasis, thereby providing new experimental platforms for systematic studies of tumor metastasis mechanisms.[108] For clinical applications, bioprinted patient-derived tumor organoids have already

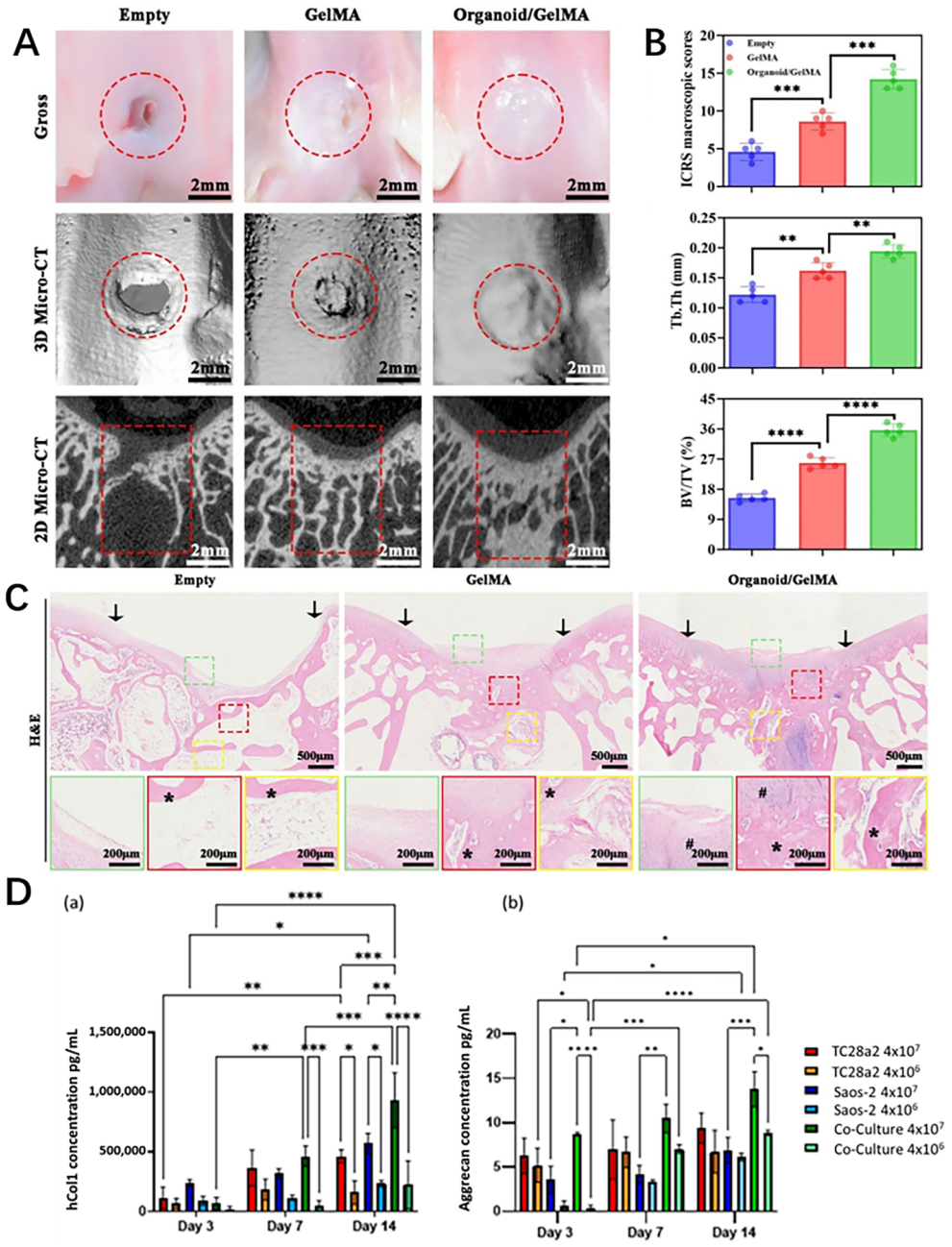

Figure 7. *In vivo* osteochondral defect repair efficacy of cartilage organoid-laden gelatin methacryloyl (GelMA) constructs and *in vitro* co-culture matrix secretion performance. (A) Organoid/GelMA group: the defect region was completely filled, and the regenerated surface was smooth and seamlessly integrated with the surrounding cartilage tissue. A large number of newly formed trabeculae with relatively uniform thickness were observed, exhibiting excellent integration with host bone tissue. (B) The International Cartilage Repair Society (ICRS) scores, trabecular thickness, and bone volume fraction in the organoid/GelMA group were all significantly greater than those in the control group ($p < 0.01$ to $p < 0.0001$). (C) Organoid/GelMA group: the three-layered structure consisting of the cartilage layer, transitional layer, and subchondral bone layer remained intact and was well integrated with the surrounding tissues. Control group: severe structural defects were clearly observed. Scale bar: 500 μm/200 μm. Reprinted with permission from Chen *et al.*[143] Copyright © 2025, The Author(s). (D) Enzyme-linked immunosorbent assay analysis of supernatants showing the concentrations of (a) human type I collagen and (b) aggrecan, comparing monoculture and co-culture groups with high and low cell densities. Reprinted with permission from Bowes *et al.*[144]

been used for rapid clinical anticancer drug screening, providing important guidance for designing personalized treatment strategies for cancer patients. Under perfusion culture conditions, Mao and coworkers established a 3D co-culture model integrating SK-N-AS neuroblastoma cells and HUVECs. Nascent peritumoral microvessels emerged as early as day 10 of cultivation, with progressive maturation of the microvascular network evident by day 21 (Figure 8A). By day 14, angiogenic sprouting from endothelialized primary vascular conduits was evident, as neovessels extended into the surrounding matrix, crossed the vascular barrier, and projected toward the tumor compartment (Figure 8B). By the end of the 21-day culture period, tumor aggregates proximal to the primary vascular channels had formed protrusive intercellular junctions with the vascular lumen, and the fully arborized microvascular network had completely ensheathed the tumor spheroids (Figure 8C). This biomimetic platform faithfully recapitulates core pathophysiological processes underlying tumor angiogenesis and distant metastasis, offering a robust experimental framework for systematic interrogation of tumor metastatic mechanisms.[109,147]

4.5 Kidney organoids

The kidney is a highly heterogeneous parenchymal organ with multistage filtration and tubular processing. The nephron serves as its fundamental functional unit and comprises intricate anatomical structures such as glomeruli and renal tubules. Consequently, the kidney has long been a major research target in tissue engineering and bioprinting. Current studies have achieved preliminary spatial organization of multiple cellular components and partial recapitulation of renal physiological functions. For example, extrusion-based bioprinting has been used to combine renal epithelial cells with hydrogel scaffolds to construct biomimetic renal tubular models with tubular topologies, partially reproducing transmembrane transport functions.[148] Using microfluidic coaxial bioprinting, metanephric mesenchymal cells and ureteric bud progenitor cells derived from human iPSCs can be encapsulated within core-shell fibers. Cell viability exceeds 90% at 24 h after printing, and the differentiated constructs exhibit appropriate drug-response capabilities.[149] At the bioink level, a photocrosslinkable bioink derived from porcine kidney decellularized extracellular matrix is compatible with both extrusion-based printing and DLP technologies, demonstrating markedly superior structural fidelity and renal microenvironment mimicry compared with conventional GelMA bioinks. In addition, stiffness-tunable self-assembling peptide hydrogel scaffolds can upregulate the expression of podocyte maturation markers through mechanotransduction pathways while reducing nonspecific cellular differentiation, thereby promoting the functional maturation of kidney organoids.[150] From the perspective of technological requirements, bioprinting of kidney organoids imposes several distinctive demands on both fabrication processes and material systems. First, high-resolution fabrication and the ability to construct complex tubular architectures are essential. Renal tubules have diameters of only several tens of micrometers, while the glomerular capillary network is even more intricate, requiring printing resolutions on the order of 50 μm together with the capability to fabricate continuously curved hollow structures. Although DLP-based photopolymerization printing offers superior fabrication precision, challenges remain in overcoming the reduction in printing accuracy caused by light scattering in high-cell-density systems. Second, the construction of hierarchical vascular networks is critical. As a highly perfused organ, the kidney requires the simultaneous fabrication of multiscale vascular structures ranging from large vessel branches and interlobular vessels to glomerular capillary networks. The predominant approach currently involves creating hollow channels using sacrificial materials, followed by endothelialization through endothelial cell seeding. Third, precise spatial positioning of multiple cell populations is required. Podocytes, renal tubular epithelial cells, vascular endothelial cells, mesangial cells, and other functional cell types must be accurately arranged during printing. The precision of cell placement directly influences the efficiency of nephron formation and the structural integrity of the resulting constructs. Finally, bioinks must provide a kidney-specific microenvironment. Generic hydrogel materials cannot fully recapitulate the biochemical signals necessary for kidney development and maturation. Consequently, organ-specific decellularized extracellular matrix-based bioinks have emerged as a major development trend, with the principal challenge being the optimization of printability while preserving biological activity.[151]

4.6. Brain organoids

Brain organoid bioprinting aims to construct functional neural networks and recapitulate cortical laminar structures, with particular emphasis on neural microenvironment regulation and neural circuit reconstruction. Functional neural tissues exhibiting electrophysiological activity have already been generated. Through horizontal layer-by-layer printing, PSC-derived neurons encapsulated within low-stiffness bioinks can form both intra-layer and inter-layer synaptic connections, establishing neural networks capable of neurotransmitter transmission. Furthermore, six-layer GelMA constructs containing cortical neurons use built-in perfusable channels to maintain mass transport

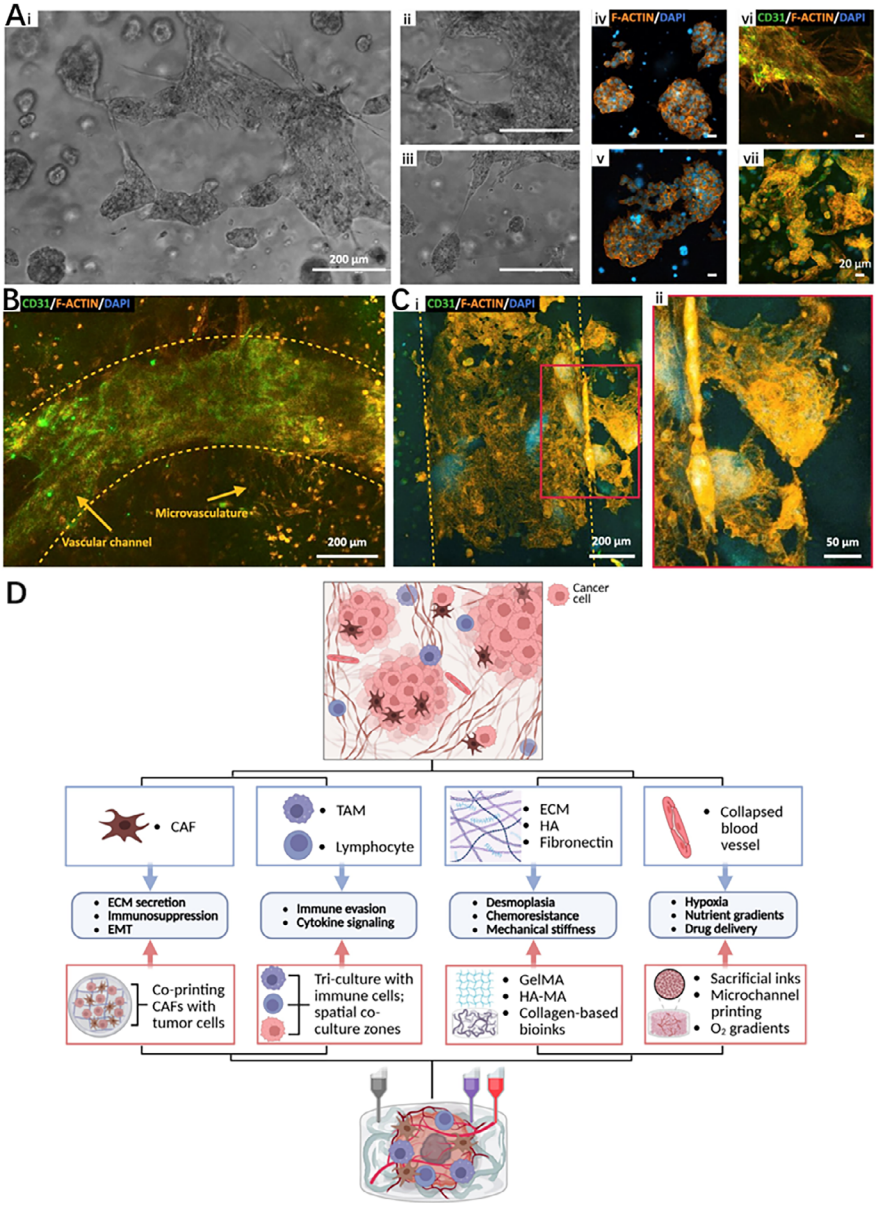

Figure 8. 3D-bioprinted perfusable vascularized tumor model and multicellular co-culture strategy for tumor microenvironment reconstruction. (A) 3D co-culture model of SK-N-AS neuroblastoma cells and HUVECs under perfusion culture conditions. On day 10 (i–iii), microvessel formation around tumor aggregates (> 500 μm) was observed, whereas by day 21 (iv–vii), the microvascular network had further matured. Scale bar: 200 μm/20 μm. (B) Under perfusion culture on day 14, endothelialized primary vascular channels generated neovessel sprouts into the surrounding GelMA matrix (tumor niche matrix), crossing the vascular barrier and extending toward the tumor region. Scale bar: 200 μm. (C) On day 21, SK-N-AS tumor aggregates located near the primary vascular channels formed connections with the vascular lumen through protrusive structures, while the microvascular network completely enclosed the tumor spheroids. Scale bar: 200 μm/50 μm. Reprinted with permission from Maggiotto *et al.*[108] (D) Illustration of the multicellular co-culture strategy at the cellular construction level, showing the correspondence between key cellular components of the pancreatic ductal adenocarcinoma (PDAC) tumor microenvironment and their related 3D bioprinting technologies: tumor cells → spatial compartmentalized co-culture printing; CAFs → co-printing with ECM-mimicking bioinks such as GelMA/HAMA; TAMs and immune cells → tri-culture systems; vasculature → printing of perfusable microchannels using sacrificial bioinks. Reprinted with permission from Vaskovich-Koubi *et al.*[106] Copyright © 2025, The Author(s). Abbreviations: CAF: Cancer-associated fibroblast; ECM: Extracellular matrix; EMT: Epithelial–mesenchymal transition; GelMA: Gelatin methacryloyl; HA: Hyaluronic acid; HA-MA: Methacrylated hyaluronic acid; HUVEC: Human umbilical vein endothelial cell; TAM: Tumor-associated macrophage.

and have been applied in studies of neural development and central nervous system drug screening.[36,152] At the level of developmental regulation, 3D-printed scaffolds can modulate the growth patterns, cellular regionalization, and vascular co-culture of brain organoids through modulus matching and spatial confinement. Soft matrices with mechanical properties comparable to those of the developing human brain promote cortical organoid lamination and normalization of gene expression profiles. Moreover, multimaterial bioprinting enables the fabrication of layered blood-brain barrier models incorporating endothelial cells, pericytes, and astrocytes, overcoming the limitations of conventional Transwell models that lack 3D architecture and providing a platform suitable for drug permeability evaluation. The biological characteristics of brain organoids impose requirements distinct from those of other solid organs. First, low-shear-force printing processes are essential. Neurons are highly sensitive to mechanical shear stress, and excessive shear during extrusion may cause axonal damage and cell death. Therefore, low-shear technologies such as inkjet bioprinting, LAB, and microfluidic coaxial bioprinting are preferred, often in combination with bioinks exhibiting excellent shear-thinning properties. Second, ultra-soft matrix compatibility is required. Brain tissue possesses an elastic modulus of only 0.1–1 kPa, substantially lower than that of most solid organs, necessitating bioinks with extremely low post-crosslinking stiffness. Conventional GelMA typically must be used at concentrations below 5%, or alternatively replaced by neural tissue-derived decellularized extracellular matrix bioinks. Excessive matrix stiffness markedly inhibits neurite extension and neural network formation. Third, spatial organization and guidance of neural pathways are crucial. Printing trajectories must be designed to direct neuronal alignment and axonal growth, thereby establishing neural circuits with defined connectivity patterns rather than random cellular aggregates. Fourth, optimization of interlayer integration is necessary. Conventional vertical layer-by-layer printing often disrupts interlayer connectivity, whereas horizontal stacking and embedded suspension printing are more conducive to neurite extension across layers and the formation of continuous 3D neural networks.[153]

4.7. Cardiac organoids

Cardiac organoid bioprinting aims to generate myocardial tissues capable of synchronized contraction, electrical coupling, and vascularized survival, making it one of the most functionally advanced directions in organoid research. In the construction of functional tissues, bioinks with cell densities reaching 10^9 cells/mL, combined with low-pressure, low-speed extrusion and electrical pulse stimulation, have been used to fabricate spontaneously beating cardiac organoids with diameters of 1–2 mm. These constructs exhibit resting beating rates of 60–80 beats per minute, contractile forces corresponding to 30%–42% of those of native myocardium, and *in vitro* survival rates exceeding 90%.[154] For the fabrication of complex structures, progressive suspension bioprinting exploits the dual characteristics of microgel-based biphasic bioinks to produce ventricular models containing intricate perfusable vascular networks while maintaining both external geometric accuracy and internal vascular complexity. By integrating computationally designed vascular networks containing millions of branches with sacrificial-material strategies, vascularized cardiac tissues with centimeter-scale thickness can be generated, achieving deep-cell survival rates of up to 90%.[155] In terms of fabrication strategy, development-inspired *in situ* differentiation approaches directly print undifferentiated PSCs and subsequently induce mesodermal and cardiomyocyte differentiation through temporally controlled modulation of the Wnt signaling pathway. This enables cardiomyocytes and fibroblasts to originate from a common progenitor cell pool, more closely resembling natural embryonic cardiac development.[154] The functional characteristics of cardiac organoids impose several specific requirements on bioprinting technologies and biomaterial systems. First, the ability to achieve directional cellular organization and anisotropic tissue construction is essential. Native myocardium exhibits a highly ordered helical architecture that directly determines contractile efficiency. Therefore, strategies such as aligned extrusion, electric- or magnetic-field-assisted printing, and microstructure-guided patterning are required to direct cardiomyocyte alignment and generate anisotropic myocardial fiber architectures. Second, conditions supporting electrical coupling and synchronized contraction must be established. Cardiomyocytes rely on gap junction proteins, particularly connexin-43, for synchronized electrical signal propagation. Functional electrical coupling networks require intercellular distances below 20 μm and high cell-density organization; low-density printing generally fails to establish effective electromechanical integration. Third, dynamic matching of mechanical properties is required. Because myocardial tissue experiences continuous mechanical loading, bioinks should possess elastic moduli in the range of 10–50 kPa together with excellent fatigue resistance, providing structural support without restricting myocardial contraction. Abnormal matrix stiffness can significantly impair cardiomyocyte maturation. Fourth, the survival of thick tissues depends on effective perfusion. Due to the high metabolic demand of cardiac tissue, thick constructs are prone to central necrosis. Consequently,

perfusable vascular networks with intervascular spacing not exceeding 200 μm (the oxygen diffusion limit) must be established, placing stringent requirements on internal channel design and sacrificial-material fabrication strategies (Table 5).[156]

Table 5. Bioprinting adaptation requirements and translational challenges for different organoid types

Organoid type	Recommended printing cell density	Shear damage tolerance characteristics	Printable material compatibility	Vascularization requirements and implementation difficulty	Clinical translation challenges	References
Liver organoids	1×10^7–5×10^7 cells/mL. Multicellular zonal co-printing of hepatocytes, hepatic stellate cells, cholangiocytes, and vascular endothelial cells is employed to recapitulate the functional zonation of hepatic lobules.	Moderate tolerance. Primary stem cells and induced pluripotent stem cell-derived hepatic progenitor cells are sensitive to shear stress. Excessive shear significantly reduces albumin secretion and CYP450 metabolic activity, thereby impairing functional maturation.	Broad compatibility based primarily on natural soft hydrogels. Common systems include collagen, Matrigel, alginate, and hyaluronic acid. These materials are compatible with inkjet, extrusion-based, and photocuring printing technologies and support the fabrication of biomimetic hepatic lobule structures.	Very high demand; very high difficulty. Simultaneous construction of portal tract–central vein vascular trunks and sinusoidal microvascular networks is required to overcome the 200 μm oxygen diffusion limit, which remains the primary bottleneck for long-term culture of large organoids.	Difficulty in maintaining long-term hepatic function *in vitro*; insufficient standardization of hepatic lobule polarity; challenges in constructing integrated vascular–biliary systems; batch-to-batch consistency remains inadequate for clinical quality control.	23,157-159
Intestinal organoids	5×10^6–2×10^7 cells/mL. Epithelial cells, stromal fibroblasts, and vascular endothelial cells are arranged in a layered manner, with a relatively high cell density in the mucosal layer to ensure barrier integrity.	Relatively low tolerance. Intestinal epithelial cells are sensitive to shear stress. Excessive shear can disrupt tight junctions, decrease transepithelial electrical resistance, and compromise epithelial barrier function.	Primarily natural hydrogels with gradient-modulus designs. Collagen-, Matrigel-, and alginate-based systems are commonly used. Soft inner matrices support epithelial polarization, whereas mechanically reinforced outer matrices maintain tubular morphology and are suitable for coaxial extrusion printing.	Relatively high demand; relatively high difficulty. Submucosal microvascular networks are required to support epithelial nutrition and mass transport. Although less complex than hepatic vascular systems, they must conform to tubular topology and crypt–villus architecture.	Long-term maintenance of crypt–villus topology remains challenging; microbiota–host co-culture systems lack stability; physiological simulation of intestinal peristalsis is absent; *in vivo* integration following transplantation requires further validation.	135,160-163

(*Cont'd...*)

Table 5. (*Continued*)

Organoid type	Recommended printing cell density	Shear damage tolerance characteristics	Printable material compatibility	Vascularization requirements and implementation difficulty	Clinical translation challenges	References
Osteochondral organoids	Cartilage layer: 1 × 107–3 × 107 cells/mL; Bone layer: 5 × 106–1 × 107 cells/mL. A gradient density design is adopted, with a high cell density in the cartilage layer to promote extracellular matrix secretion and reserved mineralization space in the bone layer.	High tolerance. Mesenchymal stem cells and mature chondrocytes exhibit significantly greater shear resistance than epithelial cells and are compatible with extrusion-based printing of high-viscosity materials.	The broadest compatibility, covering materials from soft hydrogels to rigid scaffolds. The cartilage layer typically employs gelatin methacryloyl (GelMA), hyaluronic acid, and collagen hydrogels, whereas the bone layer utilizes polyester–ceramic composite systems such as polycaprolactone/polylactic acid combined with hydroxyapatite, enabling integrated gradient printing.	Gradient-dependent requirement; moderate difficulty. The cartilage layer should maintain an avascular microenvironment to prevent pathological calcification, whereas the subchondral bone layer requires efficient vascularization. Precise regulation of vascular gradients at the interface remains the key challenge.	Insufficient osteochondral interface integration; regenerated hyaline cartilage exhibits inferior mechanical strength compared with native tissue; long-term stability in load-bearing sites lacks large-scale clinical evidence; immunogenicity control remains challenging.	[164-166]
Tumor organoids	1 × 106–1 × 107 cells/mL. The composition varies substantially among tumor types and generally includes spatially organized tumor cells, cancer-associated fibroblasts, immune cells, and endothelial cells.	High tolerance. Tumor cells possess strong stress resistance and exhibit substantially greater tolerance to shear stress than normal functional cells, making them compatible with various printing technologies.	Extremely broad compatibility with tunable matrix stiffness. Soft systems (collagen–Matrigel) are suitable for tumors with loose stroma, such as hepatocellular carcinoma, whereas stiffer systems (fibrin–hyaluronic acid) better mimic desmoplastic tumors such as pancreatic cancer.	Moderately high demand; moderately high difficulty. The focus is on recapitulating tumor vascular barriers, angiogenesis, and invasion interfaces rather than merely providing nutrient supply, thereby supporting studies of drug penetration and tumor metastasis.	Low expansion efficiency of patient-derived primary cells; difficulty in standardized recapitulation of intratumoral heterogeneity; incomplete reconstruction of the immune zmicroenvironment; predictive accuracy of drug-response testing requires further improvement.	[167-169]
Kidney organoids	5 × 106–2 × 107 cells/mL. Precise spatial positioning of podocytes, renal tubular epithelial cells, endothelial cells, and mesangial cells is required to recapitulate nephron architecture.	Extremely low tolerance. Podocytes and renal tubular epithelial cells are highly sensitive to shear stress. Excessive shear can disrupt cell polarity and impair the structural integrity of filtration units, necessitating low-shear printing techniques.	Relatively narrow compatibility, relying primarily on organ-specific bioinks. Representative systems include photocrosslinkable kidney decellularized extracellular matrix bioinks, low-concentration GelMA, and self-assembling peptide hydrogels, which are compatible with photocuring and microfluidic printing technologies.	Very high demand; very high difficulty. Glomerular capillary loops and peritubular vascular networks must be constructed simultaneously. The precision required at the vascular–parenchymal interface is among the highest of all organoid types.	Generation of fully functional nephrons remains difficult; filtration and reabsorption functions are insufficiently mature; vascular network precision remains below physiological levels; functional integration after transplantation is limited.	[150,170-172]

(*Cont'd...*)

Table 5. (*Continued*)

Organoid type	Recommended printing cell density	Shear damage tolerance characteristics	Printable material compatibility	Vascularization requirements and implementation difficulty	Clinical translation challenges	References
Brain organoids	1 × 107–3 × 107 cells/mL. Layered arrangement of neurons, astrocytes, and endothelial cells is required to mimic the ultra-soft microenvironment of brain tissue.	Extremely low tolerance. Neuronal axons are highly sensitive to shear stress. Shear generated during extrusion can induce apoptosis, axonal rupture, and neural circuit disruption. Therefore, low-shear printing technologies are preferred.	The narrowest compatibility, restricted to ultra-soft matrices. Common materials include low-concentration GelMA (<5%), neural tissue-derived decellularized extracellular matrix bioinks, and silk fibroin hydrogels, which are mainly compatible with inkjet, laser-assisted, and low-shear extrusion bioprinting.	High demand; high difficulty. Blood–brain barrier models and microvascular networks must be established simultaneously to support deep-neuron survival while preserving the three-dimensional continuity of neural circuits.	Neural circuits exhibit limited functional maturation; controllability of cortical lamination remains poor; blood–brain barrier functionality is incomplete; electrophysiological properties differ substantially from those of native brain tissue.	[173-175]
Cardiac organoids	5 × 107–1 × 10^8 cells/mL. The highest among all organoid types; high-density cardiomyocyte organization is essential for achieving intercellular electrical coupling and synchronized global contraction.	Relatively low tolerance. Cardiomyocytes are sensitive to shear stress. Excessive shear can disrupt sarcomere organization, reduce connexin-43 expression, and impair electrical coupling and synchronized contraction.	Moderate compatibility requiring strict matching of myocardial mechanical properties. Typical systems include GelMA-, collagen-, and alginate-based composites. The elastic modulus should be maintained within 10–50 kPa and is compatible with extrusion and suspension printing technologies.	Very high demand; very high difficulty. Due to the high metabolic demand of myocardial tissue, dense perfusable vascular networks with intervascular spacing below 200 μm are required. Central necrosis readily develops in centimeter-scale tissues, representing a major technical challenge.	Achieving mature synchronized global contraction remains challenging; tissue-wide electrical coupling is difficult to establish; long-term survival of vascularized thick tissues is limited; controllability of electrophysiological integration risks after transplantation remains insufficient.	[176-179]

5. Technical challenges and solutions

5.1. Balancing resolution and complex structural fabrication

A fundamental trade-off persists across all bioprinting modalities: high resolution is often achieved at the expense of structural scale and material compatibility. Inkjet- and photopolymerization-based systems achieve micron- to submicron-level precision but exhibit poor compatibility with high-cell-density bioinks, making them unsuitable for fabricating large-volume 3D constructs. Extrusion-based bioprinting supports large-scale, multi-material fabrication, but its resolution is constrained by nozzle diameter, typically limiting feature sizes to above 100 μm. This prevents the accurate replication of *in vivo* microanatomical structures such as hepatic sinusoids, intestinal crypt–villus units, and aligned myocardial fibers.[180] Furthermore, improvements in resolution often rely on rheological optimization of bioinks; however, non-physiological chemical modifications introduced to improve printability may compromise cell viability and biological function, creating a conflict between fabrication precision and cellular bioactivity.[50] Three mainstream strategies have been developed to address this trade-off. First, hybrid printing systems integrate complementary technologies—for example, combining extrusion-based macro-scaffold prefabrication with *in situ* photopolymerization for microscale structural refinement—to achieve cross-scale integrated fabrication of organoid constructs.[181] Second, rheologically optimized bioinks with shear-thinning and rapid self-solidification properties are engineered through nanomaterial doping,

dynamic covalent bonding, or supramolecular assembly. These formulations support high-resolution printing through fine nozzles while maintaining structural stability and biocompatibility after deposition.[182] Third, AI-assisted printing path planning enables region-specific parameter optimization: functional microregions use high-resolution, low-speed modes, whereas structural support regions use larger filaments at higher speeds, thereby balancing precision, fabrication efficiency, and cell viability.[51]

5.2. Cell viability and functional maintenance

Mechanical stress and environmental stimuli during printing universally impair cell viability, although the mechanisms of damage differ among printing modalities. Extrusion systems impose sustained shear stress through fine nozzles; inkjet systems generate droplet ejection impact forces and thermal bubble-induced temperature fluctuations; and photopolymerization systems present risks of photoinitiator cytotoxicity and light-induced photodamage. Across mainstream technologies, post-printing cell viability typically ranges from 70% to 90% and can decrease to below 50% in certain high-resolution protocols.[9] Beyond acute cell damage, multicellular co-printing presents additional challenges. Differences in culture requirements, proliferation rates, and differentiation timelines among various cell types make it difficult to support the simultaneous survival and functional maturation of all cell populations, thereby limiting the efficiency of complex organoid fabrication.[183]

Three complementary strategies are widely adopted to overcome these challenges. First, cell-friendly system optimization incorporates constant temperature and humidity control together with full-process sterile modules into printing equipment, minimizing viability loss caused by environmental fluctuations and contamination.[52] Second, biomimetic bioink design incorporates cell-adhesive peptides (e.g., RGD, YIGSR), lineage-specific inductive factors, and nutritional components to recreate native extracellular matrix microenvironments, thereby supporting cell adhesion, stemness maintenance, and directed functional maturation after printing.[184] Third, dynamic perfusion culture systems integrating bioreactors or microfluidic chips provide continuous nutrient supply and waste removal while applying physiologically relevant mechanical stimuli (fluid shear stress and cyclic stretch) to promote functional maturation—for example, enhancing sarcomere organization in cardiac organoids and metabolic activity in liver organoids.[185]

5.3. Construction of vascular networks and perfusion systems

The lack of hierarchical, perfusable microvascular networks remains the primary bottleneck limiting the fabrication of large-scale organoids. Native vasculature possesses a multilevel branching architecture with terminal capillaries measuring only 5–10 μm in diameter, which cannot yet be reliably reproduced using current printing technologies. As a result, oxygen and nutrient diffusion cannot adequately reach the core of constructs thicker than 200 μm, leading to irreversible ischemic necrosis and restricting the long-term culture of large-volume organoids.[186] In addition, existing approaches are unable to fully recapitulate functional vascular-parenchymal interfaces, such as hepatic sinusoids and glomerular capillary loops, where specialized material exchange and paracrine signaling occur.[187]

Three primary vascularization strategies have been established. First, sacrificial templating uses biodegradable materials printed into predefined vascular patterns, which are subsequently embedded within cell-laden hydrogels. Mild dissolution of the template creates hollow perfusable channels, which are then endothelialized to form functional vascular conduits.[188] Second, coaxial bioprinting fabricates core-shell structures in a single step, in which the core forms perfusable channels while the shell contains endothelial and parenchymal cells, eliminating the need for secondary cell seeding and improving vascularization efficiency.[189] Third, cell self-assembly-based microvascularization co-encapsulates endothelial cells, smooth muscle cells, and pericytes in bioinks containing gradient angiogenic factors (VEGF and angiopoietin-1). The spontaneously formed capillary networks subsequently connect with printed large-diameter channels, generating hierarchical "macrovessel-microvessel" architectures that support the long-term culture of large organoids.[190]

5.4. Cost and accessibility

High equipment and material costs remain the major barrier to clinical translation and large-scale adoption. High-end commercial bioprinters cost hundreds of thousands to millions of Chinese yuan, while GMP-grade clinical systems may exceed tens of millions of Chinese yuan, placing them beyond the reach of most research and clinical institutions. Bioink raw materials—including recombinant cytokines (e.g., R-spondin1 and Noggin), clinical-grade matrices, and modified biomacromolecules—also increase the cost of each organoid to hundreds of Chinese yuan, thereby limiting high-throughput applications.[191,192] In addition, the entire workflow depends on highly trained multidisciplinary personnel, and inadequate process standardization leads to poor reproducibility across laboratories, further hindering widespread implementation.[193]

Two complementary approaches are currently being pursued to improve accessibility. First, low-cost

biomaterial development focuses on using plant-derived recombinant proteins and defined universal composite bioinks to replace expensive animal-derived matrices and tissue-specific formulations, thereby reducing material costs while maintaining biological performance.[194] Second, equipment democratization promotes simplified desktop bioprinters equipped with integrated standardized protocols, together with localized manufacturing, to reduce dependence on specialized commercial suppliers and lower procurement costs.[195] For clinical applications, regional centralized organoid manufacturing centers can enable intensive utilization of equipment and technical expertise, providing standardized drug screening services to surrounding medical institutions while reducing the per-unit cost.[196]

6. Future prospects of bioprinting applications

6.1. Tissue and organ regeneration and repair

In response to the global shortage of donor organs and the increasing demand for regenerative therapies, bioprinting is expected to advance toward functional, minimally invasive, and scalable clinical translation.[197] Near-term development will focus on off-the-shelf osteochondral integrated grafts and vascularized solid organ patches (liver and myocardium) with patient-matched immunocompatibility, addressing key limitations of traditional transplantation such as immune rejection and size mismatch. In the long term, disruptive technologies such as deep-tissue *in vivo* sono-printing may enable non-invasive *in situ* fabrication directly within lesion sites, shifting the paradigm from "*ex vivo* fabrication + surgical implantation" to "*in vivo* on-demand manufacturing" while minimizing surgical trauma.[198]

6.2. Disease modeling and precision medicine

For oncology and rare disease research, bioprinting is expected to enable standardized, high-throughput manufacturing of patient-derived organoids that faithfully recapitulate tumor heterogeneity and rare disease pathologies, thereby overcoming the interspecies differences and sample limitations associated with traditional models.[199] The integration of bioprinted patient-derived organoids with multi-organ-on-a-chip platforms will further support systematic investigations of disease progression and off-target effects while enabling personalized drug-response prediction. This advancement will promote the transition from empirical treatment to predictive precision medicine, providing tailored therapeutic strategies for patients with advanced cancer or rare genetic disorders.

6.3. Drug development and toxicological evaluation

Bioprinted human organoid models are expected to gradually replace animal testing as the primary platform for preclinical efficacy and toxicity evaluation, addressing the long-standing challenges of lengthy research and development (R&D) cycles, high costs, and low clinical translation rates. Standardized large-scale production of multi-organ-on-a-chip systems will enable comprehensive simulation of drug absorption, distribution, metabolism, and excretion processes in the human body. Combined with high-throughput screening workflows, this approach will substantially shorten drug development timelines, reduce R&D costs, and better align with the 3Rs (replacement, reduction, refinement) principle for more efficient, accurate, and ethical drug discovery.[200]

6.4. Innovation and development of bioinks

Bioink innovation will shift from basic printability optimization toward clinically compliant, functionally integrated next-generation materials, addressing the translational bottlenecks of animal-derived matrices. Xenogeneic-free bioinks will become a core development direction. Plant-derived composite systems (e.g., aloe vera-based hydrogels with Lap and GelMA) eliminate animal pathogen risks and immune concerns while retaining excellent printability and osteoinductive activity, providing a xeno-free alternative for clinical-grade bone organoid fabrication (Figure 9G).[201] In the field of neural tissue engineering, Yeh *et al.*[202] developed a conductive SilMA/pectin/MXene-soy phospholipid bioink (Figure 9A–9C). Soy phospholipid modification effectively resolved the aggregation problem of MXene, while the mechanical properties of the hydrogel closely resembled those of native spinal cord tissue. Under continuous electrical stimulation at 300 μA, the neuronal differentiation rate of encapsulated neural stem cells reached 87.57%, accompanied by significantly enhanced synaptic function, thereby providing a new strategy for spinal cord injury repair. In seafood biotechnology research, novel bioink systems have also been developed. These newly engineered bioinks demonstrated excellent printability and biocompatibility, enabling the successful fabrication of cell-fat composite squid-like cultured seafood prototypes. For the first time, fully plant/algae-derived materials were used to fabricate cultured seafood products possessing both high cell viability and authentic seafood flavor, thereby providing a new technological route for the precise manufacturing of sustainable cultured seafood (Figure 9D–9F).[203]

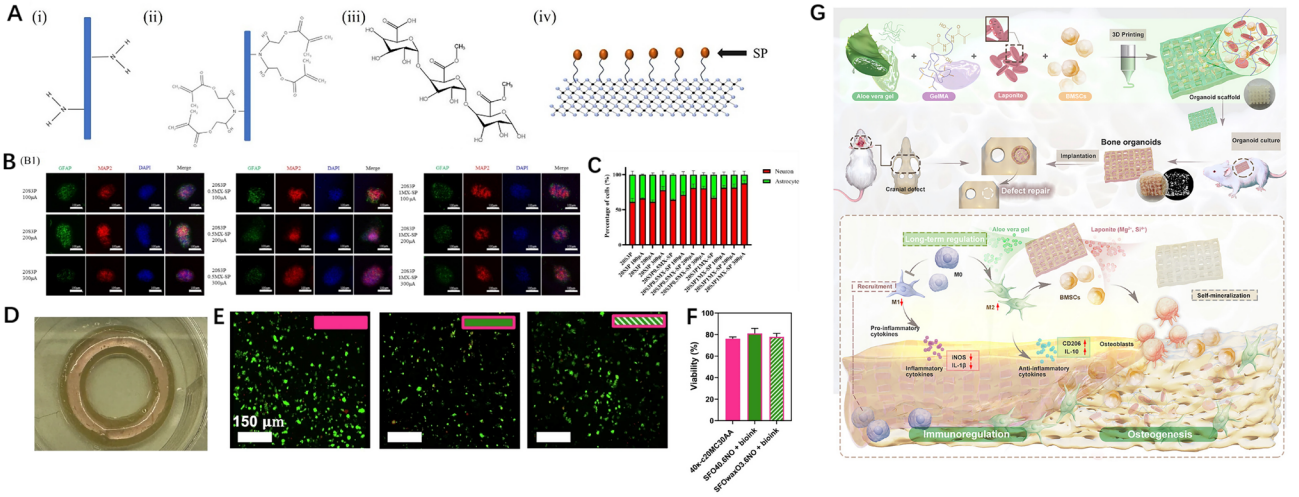

Figure 9. Design and application scenarios of three novel functional bioink systems for neural engineering, cultured seafood and bone regeneration. (A) Illustration of four core materials. (i) Silk fibroin (SF): natural protein scaffold. (ii) SilMA: methacrylate double bonds introduced into SF lysine residues through a ring-opening reaction with glycidyl methacrylate. (iii) Pectin: an anionic polysaccharide providing shear-thinning behavior. (iv) MXene-SP: MXene nanosheets coated with soy phospholipid (SP). (B–C) Immunofluorescence staining after daily electrical stimulation for 10 min over 5 consecutive days. The neuronal proportion increased progressively with increasing current intensity. In the 20S3P1MX-SP + 300 μA group, the neuronal proportion reached 87.57 ± 3.83%, whereas the astrocyte proportion was significantly decreased. Under identical current conditions, the MXene-SP group exhibited a markedly higher neuronal proportion than the MXene-free group. Scale bar: 100 μm. Reprinted with permission from Yeh *et al.*[202] (D) Actual 3D-bioprinted hybrid construct. (E) Confocal live/dead staining image obtained after 15 days of culture. Scale bar: 150 μm. (F) Quantitative analysis of cell viability: the control group (κ-CAM only) exhibited 76.14% viability, the SFO40.6NO hybrid group showed 81.10%, and the SFOwaxO3.6NO hybrid group displayed 77.87%, with no statistically significant differences observed among the three groups. Reprinted with permission from Marques *et al.*[203] Copyright © 2025, The Author(s). (G) A composite bioink consisting of aloe vera gel, GelMA, and Laponite nanoclay loaded with bone marrow mesenchymal stem cells (BMSCs) was used to fabricate biomimetic scaffolds through 3D bioprinting, followed by *in vitro* culture to generate functional bone organoids.[201] Reprinted with permission from Zhang *et al.*[201] Copyright © 2026, Elsevier Inc.

6.5. Artificial intelligence-driven and intelligent bioprinting

6.5.1. Intelligent prediction and high-throughput screening of bioink formulations

Bioinks are the core carriers that determine the printing fidelity and cellular viability of bioprinted constructs. Their formulation development requires the simultaneous optimization of multiple parameters, including rheological properties, mechanical strength, degradation kinetics, and biocompatibility. Conventional trial-and-error approaches based on single-variable experimentation are constrained by parameter coupling effects and are characterized by long development cycles, high material consumption, and low optimization efficiency. To meet the need for multi-objective formulation optimization, small-sample learning algorithms such as Bayesian optimization and Gaussian process models can use existing experimental datasets to establish quantitative relationships among material composition, printing performance, and biological outcomes. Through a closed-loop strategy of prediction, validation, and iteration, these approaches can rapidly identify optimal formulations that combine excellent printability with desirable biological functionality. Compared with conventional screening methods, the required experimental scale can be reduced by more than an order of magnitude, significantly lowering development costs and resource consumption. In the development of GelMA and methacrylated hyaluronic acid-based composite hydrogels, this approach enables the simultaneous optimization of key parameters such as viscosity, yield stress, swelling ratio, and crosslinking kinetics, thereby improving cell viability while maintaining structural fidelity. Its optimization efficiency has been shown to exceed that of traditional experimental design methods.[204] When integrated with high-throughput droplet printing and microfluidic technologies, computationally assisted strategies enable automated screening of bioink-cell combinations. By analyzing droplet morphology, cell distribution, and proliferation activity in real time, inefficient formulations can be automatically eliminated, substantially increasing the throughput of novel bioink development. Furthermore, simulations of material-cell interactions can be used to predict the release

kinetics of bioactive factors and cellular differentiation trajectories, providing quantitative theoretical support for the development of functional bioinks designed for immunomodulation, directed differentiation, and related applications.[205,206]

6.5.2. Dynamic simulation of organoid morphogenesis and tissue development

Organoid formation is a dynamic process driven by both cellular self-organization and microenvironmental regulation, involving multiple biological events such as cell proliferation, migration, differentiation, and extracellular matrix remodeling. Conventional experimental approaches are often unable to accurately predict long-term developmental trajectories and functional maturation outcomes and are limited by long experimental cycles, substantial inter-sample heterogeneity, and high resource consumption. Computational modeling strategies that integrate first-principles models with data-driven algorithms enable dynamic simulation of the entire process of organoid morphogenesis and tissue development, providing quantitative guidance for culture optimization and functional regulation.[207] Currently, hybrid modeling that combines physical constraints with biological principles has become the dominant technological approach in this field. First-principles models are based on fundamental mechanical, chemical, and biological laws and are capable of elucidating underlying mechanisms such as cell-matrix interactions and signaling molecule diffusion. In contrast, data-driven models learn from experimental datasets to capture complex nonlinear developmental patterns. The complementary integration of these approaches significantly improves both predictive accuracy and interpretability. Artificial intelligence virtual organoids developed using this framework can simulate 3D structural evolution, lineage differentiation, and functional maturation before *in vitro* experiments are conducted, thereby predicting developmental outcomes under different culture conditions. Such models can substantially reduce the number of experimental samples and animal studies required while also providing insights into developmental mechanisms that are difficult to observe using conventional experimental methods.[208] At the application level, high-content imaging combined with automated analytical approaches enables the automatic identification and quantification of organoid morphology, biomarker expression, and cellular distribution, facilitating high-throughput and unbiased quality assessment. In tumor organoid-based drug screening, dynamic monitoring of organoid growth, apoptosis, and drug responses enables accurate discrimination between drug-sensitive and drug-resistant phenotypes, thereby improving both screening throughput and predictive accuracy and providing technical support for personalized drug screening.[209]

6.5.3. Real-time quality control and closed-loop optimization of the bioprinting process

Process stability is a critical determinant of product consistency and clinical safety in bioprinting. However, existing quality-control strategies rely predominantly on post-process inspection, resulting in delayed defect detection and substantial waste of bioinks, cells, and experimental time. The integration of AI with computer vision and multimodal sensing technologies enables the establishment of a closed-loop quality-control framework consisting of real-time monitoring, intelligent defect recognition, and dynamic process regulation, thereby supporting *in situ* error correction and quality assurance during printing. In extrusion-based bioprinting, high-resolution imaging systems can capture each printed layer in real time. AI models based on convolutional neural networks can automatically identify common printing defects, including under-extrusion, over-extrusion, filament breakage, bubble formation, layer misalignment, and nozzle clogging, with detection accuracies exceeding 90%. Once abnormalities are detected, feedback-control mechanisms can automatically adjust parameters such as extrusion pressure, printing speed, and nozzle height to correct defects *in situ* without interrupting the printing process. This approach preserves structural fidelity while significantly reducing defect rates and material waste. For photocuring-based bioprinting, AI algorithms can compensate for cell-induced light scattering effects by optimizing mask grayscale distributions and exposure parameters, thereby mitigating precision loss caused by optical scattering. Simultaneously, ultraviolet exposure doses can be carefully regulated to maintain high cell viability while improving microstructural printing accuracy.[51] Beyond process control, AI also enables predictive maintenance of bioprinting equipment. By analyzing time-series data related to vibration, temperature, and fluid pressure, AI systems can predict risks such as nozzle blockage and mechanical drift, allowing preventive intervention before failures occur. This reduces unplanned downtime and enhances the operational stability of large-scale manufacturing systems. Such comprehensive intelligent quality-control frameworks represent a key technological foundation for translating bioprinting from laboratory-scale research to industrial and clinical applications.[210]

6.5.4. Intelligent design of personalized tissue constructs and support for clinical translation

Computer-aided tissue construct design represents one of

the earliest and most technologically mature application areas in bioprinting. Based on patient-specific medical imaging data, such as computed tomography and magnetic resonance imaging, automated image-analysis algorithms can perform lesion segmentation and 3D reconstruction of normal tissues, generating personalized scaffold models that closely match patient anatomy. Combined with the mechanical and nutrient transport requirements of the target tissue, multi-objective optimization algorithms can automatically regulate scaffold porosity, pore-size distribution, and internal topological architecture, thereby enhancing cell infiltration and nutrient diffusion while maintaining sufficient mechanical strength.[211] At the clinical translation level, computational simulation methods can support preoperative planning and prediction of implantation outcomes. By modeling the mechanical interactions between implants and host tissues, as well as the process of tissue integration, these approaches can predict regenerative outcomes and potential postoperative risks, providing quantitative guidance for surgical decision-making. Furthermore, by integrating multidimensional clinical information, including patient genotype, underlying diseases, and lifestyle factors, individualized implantation strategies can be developed. Such personalized approaches are expected to improve the precision and success rates of regenerative therapies, thereby advancing bioprinting toward the realization of precision medicine.[212]

7. Conclusion

Bioprinting has emerged as an enabling technology for the controlled fabrication of organoids, bridging advances in biomanufacturing and stem cell-derived organoid engineering. This review provides a comprehensive synthesis of recent progress in this interdisciplinary field, starting with a detailed characterization of four prevailing bioprinting modalities: inkjet-based, extrusion-based, photopolymerization-based, and laser-assisted bioprinting. For each modality, we outline its working principles, technical attributes, and representative commercial platforms and present a side-by-side comparison of core performance metrics, including spatial resolution, post-printing cell viability, and bioink compatibility. We further elaborate on the classification, biological functions, and formulation optimization strategies of bioink systems, organized around three core constituents: biomacromolecular matrices, cell populations, and bioactive factors. Building on this technical foundation, the review catalogs representative advances across seven major organoid systems—liver, intestinal, osteochondral, tumor, renal, cerebral, and cardiac organoids—and delineates the distinct technical requirements and principles for matching bioprinting modalities to each tissue context. We highlight four pervasive bottlenecks constraining further development: the fundamental trade-off between printing resolution and structural complexity, the preservation of cell viability and functional phenotypes, the construction of hierarchical perfusable vascular networks, and limitations in cost-effectiveness and scalability. Targeted mitigation strategies are discussed, including hybrid bioprinting configurations, biomimetic microenvironment engineering, and sacrificial templating approaches. Finally, we outline future research directions across five domains: tissue and organ regeneration, precision medicine platforms, preclinical drug and toxicity assessment, next-generation bioink innovation, and AI-driven biomanufacturing. This work addresses a gap in the existing literature, as previous reviews have largely focused on either bioprinting technologies or organoid fabrication methodologies in isolation. By establishing a clear framework for matching bioprinting modalities to organoid construction requirements, we define technology-selection criteria for diverse organoid applications and provide perspectives on emerging interdisciplinary areas such as AI-augmented biomanufacturing. Collectively, this review provides a conceptual reference and practical guidance for technological refinement, protocol optimization, and clinical translation in the field.

Acknowledgments

None.

Funding

This work was supported by the Dalian Science and Technology Talent Innovation Support Policy Implementation Plan (grant number 2023RJ015); Liaoning Provincial Science and Technology Program Joint Plan (grant number 2025JH2/101800314); and the Innovation and Entrepreneurship Training Program for College Students (grant number X202511258080).

Conflict of interest

The authors declare they have no conflicts of interest.

Author contributions

Conceptualization: Hui Xie, Yansong Qi
Funding acquisition: Hui Xie
Visualization: Mibo Lu
Writing–original draft: Mibo Lu
Writing–review & editing: Mibo Lu, Xu Chen, Yalei Yin

Ethics approval and consent to participate

Not applicable.

Consent for publication

Not applicable.

Availability of data

Not applicable.

References

1. Paul GM, Rezaienia A, Wen P, *et al*. Medical applications for 3D printing: recent developments. *Mo Med*. 2018;115(1):75-81.

2. Mendoza-Cerezo L, Jesús MR-R, Macías-García A, *et al*. Evolution of bioprinting and current applications. *Int J Bioprint*. 2023;9(4):742.

   doi: 10.18063/ijb.742

3. Alave Reyes-Furrer A, De Andrade S, Bachmann D, *et al*. Matrigel 3D bioprinting of contractile human skeletal muscle models recapitulating exercise and pharmacological responses. *Commun Biol*. 2021;4(1):1183.

   doi: 10.1038/s42003-021-02691-0

4. Kim W, Lee Y, Kang D, *et al*. 3D inkjet-bioprinted lung-on-a-chip. *ACS Biomater Sci Eng*. 2023;9(5):2806-2815.

   doi: 10.1021/acsbiomaterials.3c00089

5. Carberry BJ, Hergert JE, Yavitt FM, *et al*. 3D printing of sacrificial thioester elastomers using digital light processing for templating 3D organoid structures in soft biomatrices. *Biofabrication*. 2021;13(4):044104.

   doi: 10.1088/1758-5090/ac1c98

6. Keriquel V, Oliveira H, Rémy M, *et al*. In situ printing of mesenchymal stromal cells, by laser-assisted bioprinting, for in vivo bone regeneration applications. *Sci Rep*. 2017;7(1):1778.

   doi: 10.1038/s41598-017-01914-x

7. Serpe F, Nalin F, Tirelli MC, *et al*. Microfluidic 3D bioprinting of foamed fibers with controlled micromorphology. *ACS Appl Mater Interfaces*. 2025;17(9):13632-13645.

   doi: 10.1021/acsami.4c22450

8. Panwar A, Tan LP. Current status of bioinks for micro-extrusion-based 3D bioprinting. *Molecules*. 2016;21(6):685.

   doi: 10.3390/molecules21060685

9. Xu H, Liu J, Zhang Z, Xu C. A review on cell damage, viability, and functionality during 3D bioprinting. *Mil Med Res*. 2022;9(1):70.

   doi: 10.1186/s40779-022-00429-5

10. Shahabipour F, Ashammakhi N, Oskuee RK, *et al*. Key components of engineering vascularized 3-dimensional bioprinted bone constructs. *Transl Res*. 2020;216:57-76.

    doi: 10.1016/j.trsl.2019.08.010

11. Elemoso A, Shalunov G, Balakhovsky YM, *et al*. 3D bioprinting: The roller coaster ride to commercialization. *Int J Bioprint*. 2020;6(3):301.

    doi: 10.18063/ijb.v6i3.301

12. Ren Y, Yang X, Ma Z, *et al*. Developments and opportunities for 3D bioprinted organoids. *Int J Bioprint*. 2021;7(3):364.

    doi: 10.18063/ijb.v7i3.364

13. Yan HHN, Chan AS, Lai FP-L, Leung SY. Organoid cultures for cancer modeling. *Cell Stem Cell*. 2023;30(7):917-937.

    doi: 10.1016/j.stem.2023.05.012

14. Chen EP, Toksoy Z, Davis BA, Geibel JP. 3D Bioprinting of Vascularized Tissues for in vitro and in vivo Applications. *Front Bioeng Biotechnol*. 2021;9:664188.

    doi: 10.3389/fbioe.2021.664188

15. Budharaju H, Sundaramurthi D, Sethuraman S. Embedded 3D bioprinting–An emerging strategy to fabricate biomimetic & large vascularized tissue constructs. *Bioact Mater*. 2024;32:356-384.

    doi: 10.1016/j.bioactmat.2023.10.012

16. Chakraborty J, Ghosh S. Developmental biology-based 3D bioprinting: an off-the-shelf strategy to induce tissue regeneration. *ACS Biomater Sci Eng*. 2025;11(8):4552-4569.

    doi: 10.1021/acsbiomaterials.5c00213

17. Huang J, Jia S, Liang R, *et al*. Construction of organoids using bioprinting technology: a frontier exploration of cartilage repair. *J Orthop Transl*. 2025;54:37-50.

    doi: 10.1016/j.jot.2025.06.020

18. Huh D, Hamilton GA, Ingber DE. From 3D cell culture to organs-on-chips. *Trends Cell Biol*. 2011;21(12):745-754.

    doi: 10.1016/j.tcb.2011.09.005

19. Suthiwanich K, Hagiwara M. Localization of multiple hydrogels with MultiCUBE platform spatially guides 3D tissue morphogenesis in vitro. *Adv Mater Technol*. 2023;8(4):2201660.

    doi: 10.1002/admt.202201660

20. Zimmermann R, Hentschel C, Schrön F, *et al*. High resolution bioprinting of multi-component hydrogels. *Biofabrication*. 2019;11(4):045008.

    doi: 10.1088/1758-5090/ab2aa1

21. Li X, Liu B, Pei B, *et al*. Inkjet bioprinting of biomaterials. *Chem Rev*. 2020;120(19):10793-10833.

    doi: 10.1021/acs.chemrev.0c00008

22. Xu T, Gregory CA, Molnar P, *et al*. Viability and electrophysiology of neural cell structures generated by the inkjet printing method. *Biomaterials*. 2006;27(19):3580-3588.

    doi: 10.1016/j.biomaterials.2006.01.048

23. Cross-Najafi AA, Farag K, Chen AM, *et al*. The long road to develop custom-built livers: current status of 3D liver bioprinting. *Transplantation*. 2024;108(2):357-368.

    doi: 10.1097/TP.0000000000004668

24. Park JA, Lee HR, Park SY, Jung S. Self-organization of fibroblast-laden 3D collagen microstructures from inkjet-printed cell patterns. *Adv Biosyst*. 2020;4(5):1900280.

    doi: 10.1002/adbi.201900280

25. Xu H, Liu J, Zhang Z, Xu C. Cell sedimentation during 3D bioprinting: a mini review. *Bio-Des Manuf*. 2022;5(3):617-626.

    doi: 10.1007/s42242-022-00183-6

26. Kang D, Park JA, Kim W, *et al*. All-inkjet-printed 3D alveolar barrier model with physiologically relevant microarchitecture. *Adv Sci*. 2021;8(10):2004990.

    doi: 10.1002/advs.202004990

27. Summers AJ, Devadhasan JP, Gu J, *et al*. Optimization of an antibody microarray printing process using a designed experiment. *ACS Omega*. 2022;7(36):32262-32271.

    doi: 10.1021/acsomega.2c03595

28. Wüst S, Müller R, Hofmann S. Controlled positioning of cells in biomaterials-approaches towards 3D tissue printing. *J Funct Biomater*. 2011;2(3):119-154.

    doi: 10.3390/jfb2030119

29. Bolander J, Mota C, Ooi HW, *et al*. Bioinspired development of an in vitro engineered fracture callus for the treatment of critical long bone defects. *Adv Funct Mater*. 2021;31(46):2104159.

    doi: 10.1002/adfm.202104159

30. Neufeld L, Yeini E, Reisman N, *et al*. Microengineered perfusable 3D-bioprinted glioblastoma model for in vivo mimicry of tumor microenvironment. *Sci Adv*. 2021;7(34):eabi9119.

    doi: 10.1126/sciadv.abi9119

31. Tabriz AG, Hermida MA, Leslie NR, Shu W. Three-dimensional bioprinting of complex cell laden alginate hydrogel structures. *Biofabrication*. 2015;7(4):045012.

    doi: 10.1088/1758-5090/7/4/045012

32. Skardal A, Devarasetty M, Kang H-W, *et al*. A hydrogel bioink toolkit for mimicking native tissue biochemical and mechanical properties in bioprinted tissue constructs. *Acta Biomater*. 2015;25:24-34.

    doi: 10.1016/j.actbio.2015.07.030

33. Placone JK, Engler AJ. Recent advances in extrusion-based 3D printing for biomedical applications. *Adv Healthcare Mater*. 2018;7(8):1701161.

    doi: 10.1002/adhm.201701161

34. Billiet T, Gevaert E, De Schryver T, *et al*. The 3D printing of gelatin methacrylamide cell-laden tissue-engineered constructs with high cell viability. *Biomaterials*. 2014;35(1):49-62.

    doi: 10.1016/j.biomaterials.2013.09.078

35. Blaeser A, Duarte Campos DF, Puster U, *et al*. Controlling shear stress in 3D bioprinting is a key factor to balance printing resolution and stem cell integrity. *Adv Healthcare Mater*. 2016;5(3):326-333.

    doi: 10.1002/adhm.201500677

36. Yan Y, Li X, Gao Y, *et al*. 3D bioprinting of human neural tissues with functional connectivity. *Cell Stem Cell*. 2024;31(2):260-274.

    doi: 10.1016/j.stem.2023.12.009

37. Angelats Lobo D, Ginestra P. Cell bioprinting: the 3D-bioplotter™ case. *Materials*. 2019;12(23):4005.

    doi: 10.3390/ma12234005

38. Tong A, Pham QL, Abatemarco P, *et al*. Review of low-cost 3D bioprinters: state of the market and observed future trends. *SLAS Technol*. 2021;26(4):333-366.

    doi: 10.1177/24726303211020297

39. Li W, Wang M, Ma H, *et al*. Stereolithography apparatus and digital light processing-based 3D bioprinting for tissue fabrication. *iScience*. 2023;26(2):106039.

    doi: 10.1016/j.isci.2023.106039

40. Hafa L, Breideband L, Ramirez Posada L, *et al*. Light sheet-based laser patterning bioprinting produces long-term viable full-thickness skin constructs. *Adv Mater*. 2024;36(8):2306258.

    doi: 10.1002/adma.202306258

41. Li F, Li X, Dai S, *et al*. Efficient light-based bioprinting via rutin nanoparticle photoinhibitor for advanced biomedical applications. *ACS Nano*. 2024;18(33):22104-22121.

    doi: 10.1021/acsnano.4c05380

42. Gao T, Liu Z, Yin J, *et al*. Novel low-cytotoxic and highly efficient type I photoinitiators for visible LED-/sunlight-induced photopolymerization and high-precision 3D printing. *Angew Chem*. 2025;137(18):e202425598.

    doi: 10.1002/anie.202425598

43. Phogat S, Guo TJF, Thiam F, Osei ET. Establishing a 3D vascularized tri-culture model of the human airways via a digital light processing bioprinter. *Biotechnol Bioeng*. 2025;122(8):2273-2280.

    doi: 10.1002/bit.29013

44. Fleck E, Keck C, Ryszka K, *et al*. Low-viscosity polydimethylsiloxane resin for facile 3D printing of elastomeric microfluidics. *Micromachines*. 2023;14(4):773.

    doi: 10.3390/mi14040773

45. Bedir T, Sahoo SS, Kadian S, *et al*. Effect of geometric design on the mechanical performance of digital light processing (DLP)-printed microneedles. *Micromachines*. 2025;16(11):1221.

doi: 10.3390/mi16111221

46. Zhang S, Chen X, Shan M, *et al*. Convergence of 3D bioprinting and nanotechnology in tissue engineering scaffolds. *Biomimetics*. 2023;8(1):94.

doi: 10.3390/biomimetics8010094

47. Chang J, Sun X. Laser-induced forward transfer based laser bioprinting in biomedical applications. *Front Bioeng Biotechnol*. 2023;11:1255782.

doi: 10.3389/fbioe.2023.1255782

48. Finny AS, Popoola O, Andreescu S. 3D-printable nanocellulose-based functional materials: fundamentals and applications. *Nanomaterials*. 2021;11(9):2358.

doi: 10.3390/nano11092358

49. Gibriel A. Effect of target length on specificity and sensitivity of oligonucleotide microarrays: a comparison between dendrimer and modified PCR based labelling methods. *Open Biochem J*. 2014;8:11-20.

doi: 10.2174/1874091x01408010011

50. Elango J, Zamora-Ledezma C. Rheological, structural, and biological trade-offs in bioink design for 3d bioprinting. *Gels*. 2025;11(8):659.

doi: 10.3390/gels11080659

51. Chen H, Zhang B, Huang J. Recent advances and applications of artificial intelligence in 3D bioprinting. *Biophys Rev*. 2024;5(3):031301.

doi: 10.1063/5.0190208

52. Manzoli S, Merotto E, Piccoli M, *et al*. An overview of 3D bioprinting impact on cell viability: from damage assessment to protection solutions. *J Funct Biomater*. 2025;16(12):436.

doi: 10.3390/jfb16120436

53. Derman ID, Kim MH, Sarikaya MD, *et al*. Unconventional bioprinting modalities for advanced tissue biofabrication. *Biomaterials*. 2025;326:123704.

doi: 10.1016/j.biomaterials.2025.123704

54. Li Z, Li K, Zhang C, *et al*. Bioprinted organoids: an innovative engine in biomedicine. *Adv Sci*. 2025;12(33):e07317.

doi: 10.1002/advs.202507317

55. Ho Y, Liao Y, Liao L, *et al*. Advances of cell printing technology in organoid engineering. *Tissue Eng Part B Rev*. Published online June 12, 2025.

doi: 10.1089/ten.teb.2025.0048

56. Chun J, Lim KY, Kim J, *et al*. 3D bioprinting for next-generation personalized medicine. *Int J Mol Sci*. 2023;24(7):6357.

doi: 10.3390/ijms24076357

57. Unagolla JM, Jayasuriya AC. Hydrogel-based 3D bioprinting: a comprehensive review on cell-laden hydrogels, bioink formulations, and future perspectives. *Appl Mater Today*. 2020;18:100479.

doi: 10.1016/j.apmt.2019.100479

58. Saldin LT, Cramer MC, Velankar SS, *et al*. Extracellular matrix hydrogels from decellularized tissues: Structure and function. *Acta Biomater*. 2017;49:1-15.

doi: 10.1016/j.actbio.2016.11.068

59. Skardal A, Mack D, Kapetanovic E, *et al*. Bioprinted amniotic fluid-derived stem cells accelerate healing of large skin wounds. *Stem Cells Transl Med*. 2012;1(11):792-802.

doi: 10.5966/sctm.2012-0088

60. Shoulders MD, Raines RT. Collagen structure and stability. *Annu Rev Biochem*. 2009;78(1):929-958.

doi: 10.1146/annurev.biochem.77.032207.120833

61. Khew ST, Tong YW. The specific recognition of a cell binding sequence derived from type I collagen by Hep3B and L929 cells. *Biomacromolecules*. 2007;8(10):3153-3161.

doi: 10.1021/bm700587j

62. El-Sherbiny IM, Yacoub MH. Hydrogel scaffolds for tissue engineering: Progress and challenges. *Glob Cardiol Sci Pract*. 2013;2013(3):38.

doi: 10.5339/gcsp.2013.38

63. Hospodiuk M, Dey M, Sosnoski D, Ozbolat IT. The bioink: A comprehensive review on bioprintable materials. *Biotechnol Adv*. 2017;35(2):217-239.

doi: 10.1016/j.biotechadv.2016.12.006

64. Lee KY, Mooney DJ. Alginate: properties and biomedical applications. *Prog Polym Sci*. 2012;37(1):106-126.

doi: 10.1016/j.progpolymsci.2011.06.003

65. Wang L, Shelton RM, Cooper PR, *et al*. Evaluation of sodium alginate for bone marrow cell tissue engineering. *Biomaterials*. 2003;24(20):3475-3481.

doi: 10.1016/S0142-9612(03)00167-4

66. Pandit AH, Mazumdar N, Ahmad S. Periodate oxidized hyaluronic acid-based hydrogel scaffolds for tissue engineering applications. *Int J Biol Macromol*. 2019;137:853-869.

doi: 10.1016/j.ijbiomac.2019.07.014

67. Xu X, Jha AK, Harrington DA, *et al*. Hyaluronic acid-based hydrogels: from a natural polysaccharide to complex networks. *Soft Matter*. 2012;8(12):3280-3294.

doi: 10.1039/c2sm06463d

68. Pescosolido L, Schuurman W, Malda J, *et al*. Hyaluronic acid and dextran-based semi-IPN hydrogels as biomaterials for bioprinting. *Biomacromolecules*. 2011;12(5):1831-1838.

doi: 10.1021/bm200178w

69. Kleinman HK, Martin GR. Matrigel: Basement membrane matrix with biological activity. *Semin Cancer Biol*. 2005;15(5):378-386.

doi: 10.1016/j.semcancer.2005.05.004

70. Liu X, Hao M, Chen Z, *et al*. 3D bioprinted neural tissue constructs for spinal cord injury repair. *Biomaterials*. 2021;272:120771.

doi: 10.1016/j.biomaterials.2021.120771

71. Xu R, Fang Y, Zhang Z, *et al*. Recent advances in biodegradable and biocompatible synthetic polymers used in skin wound healing. *Materials*. 2023;16(15):5459.

doi: 10.3390/ma16155459

72. Zhu J. Bioactive modification of poly (ethylene glycol) hydrogels for tissue engineering. *Biomaterials*. 2010;31(17):4639-4656.

doi: 10.1016/j.biomaterials.2010.02.044

73. Qiao F, Zou Y, Bie B, Lv Y. Dual siRNA-loaded cell membrane functionalized matrix facilitates bone regeneration with angiogenesis and neurogenesis. *Small*. 2024;20(8):2307062.

doi: 10.1002/smll.202307062

74. Balla E, Daniilidis V, Karlioti G, *et al*. Poly (lactic Acid): A versatile biobased polymer for the future with multifunctional properties—From monomer synthesis, polymerization techniques and molecular weight increase to PLA applications. *Polymers*. 2021;13(11):1822.

doi: 10.3390/polym13111822

75. Alavi MS, Memarpour S, Pazhohan-Nezhad H, *et al*. Applications of poly (lactic acid) in bone tissue engineering: A review article. *Artif Organs*. 2023;47(9):1423-1430.

doi: 10.1111/aor.14612

76. Rezvani Ghomi E, Nourbakhsh N, Akbari Kenari M, *et al*. Collagen-based biomaterials for biomedical applications. *J Biomed Mater Res Part B Appl Biomater*. 2021;109(12):1986-1999.

doi: 10.1002/jbm.b.34881

77. Gao L, Wei Y, Tan Y, *et al*. Irrigating degradation properties of silk fibroin–collagen type II composite cartilage scaffold in vitro and in vivo. *Biomater Adv*. 2023;149:213389.

doi: 10.1016/j.bioadv.2023.213389

78. Dong C, Lv Y. Application of collagen scaffold in tissue engineering: recent advances and new perspectives. *Polymers*. 2016;8(2):42.

doi: 10.3390/polym8020042

79. Negrescu AM, Cimpean A. A recent insight into research pertaining to collagen-based hydrogels as dressings for chronic skin wounds. *Gels*. 2025;11(7):527.

doi: 10.3390/gels11070527

80. Axpe E, Oyen ML. Applications of alginate-based bioinks in 3D bioprinting. *Int J Mol Sci*. 2016;17(12):1976.

doi: 10.3390/ijms17121976

81. Cano-Vicent A, Tunon-Molina A, Bakshi H, *et al*. Biocompatible alginate film crosslinked with Ca2+ and Zn2+ possesses antibacterial, antiviral, and anticancer activities. *ACS Omega*. 2023;8(27):24396-24405.

doi: 10.1021/acsomega.3c01935

82. Farshidfar N, Iravani S, Varma RS. Alginate-based biomaterials in tissue engineering and regenerative medicine. *Mar Drugs*. 2023;21(3):189.

doi: 10.3390/md21030189

83. Iaconisi GN, Lunetti P, Gallo N, *et al*. Hyaluronic acid: a powerful biomolecule with wide-ranging applications—a comprehensive review. *Int J Mol Sci*. 2023;24(12):10296.

doi: 10.3390/ijms241210296

84. Shim H, Kim Y, Park KH, *et al*. Hyaluronic acid microparticles promote uniform differentiation and survival of stem cells in spheroid cultures. *ACS Omega*. 2025;10(32):36267-36275.

doi: 10.1021/acsomega.5c04198

85. Tamada Y, Takeuchi H, Suzuki N, *et al*. Cell surface expression of hyaluronan on human ovarian cancer cells inversely correlates with their adhesion to peritoneal mesothelial cells. *Tumor Biol*. 2012;33(4):1215-1222.

doi: 10.1007/s13277-012-0369-4

86. Yamagishi R, Miura S, Yabu K, *et al*. Fabrication technology of self-dissolving sodium hyaluronate gels ultrafine microneedles for medical applications with UV-curing gas-permeable mold. *Gels*. 2024;10(1):65.

doi: 10.3390/gels10010065

87. Kawase E, Nakatsuji N. Development of substrates for the culture of human pluripotent stem cells. *Biomater Sci*. 2023;11(9):2974-2987.

doi: 10.1039/D2BM01473D

88. Murphy C, Naderlinger E, Mater A, *et al*. Comparison of human recombinant protein coatings and fibroblast-ECM to Matrigel for induced pluripotent stem cell culture and renal podocyte differentiation. *ALTEX*. 2022;40(1):141-159.

doi: 10.14573/altex.2112204

89. Chen B, Cheng T, Roffler SR. Polyethylene glycol immunogenicity: theoretical, clinical, and practical aspects of anti-polyethylene glycol antibodies. *ACS Nano*. 2021;15(9):14022-14048.

doi: 10.1021/acsnano.1c05922

90. Perrino C, Lee S, Spencer ND. Quantitative comparison of the hydration capacity of surface-bound dextran and polyethylene glycol. *Langmuir*. 2024;40(27):14130-14140.

doi: 10.1021/acs.langmuir.4c01582

91. Liang J, Guo Z, Timmerman A, *et al*. Enhanced mechanical and cell adhesive properties of photo-crosslinked PEG hydrogels by incorporation of gelatin in the networks. *Biomed Mater*. 2019;14(2):024102.

doi: 10.1088/1748-605X/aaf31b

92. Maietta S, Russo T, De Santis R, *et al*. Further theoretical insight into the mechanical properties of polycaprolactone loaded with organic–inorganic hybrid fillers. *Materials*. 2018;11(2):312.

doi: 10.3390/ma11020312

93. Homaeigohar S, Boccaccini AR. Nature-derived and synthetic additives to poly (ε-caprolactone) nanofibrous systems for biomedicine; an updated overview. *Front Chem*. 2022;9:809676.

doi: 10.3389/fchem.2021.809676

94. Maduka CV, Alhaj M, Ural E, *et al*. Polylactide degradation activates immune cells by metabolic reprogramming. *Adv Sci*. 2023;10(31):2304632.

doi: 10.1002/advs.202304632

95. Naser AZ, Deiab I, Darras BM. Poly (lactic acid)(PLA) and polyhydroxyalkanoates (PHAs), green alternatives to petroleum-based plastics: a review. *RSC Adv*. 2021;11(28):17151-17196.

doi: 10.1039/D1RA02390J

96. Marquez-Curtis LA, Janowska-Wieczorek A, McGann LE, Elliott JAW. Mesenchymal stromal cells derived from various tissues: Biological, clinical and cryopreservation aspects. *Cryobiology*. 2015;71(2):181-197.

doi: 10.1016/j.cryobiol.2015.07.003

97. Wagner W, Ho AD, Zenke M. Different facets of aging in human mesenchymal stem cells. *Tissue Eng Part B Rev*. 2010;16(4):445-453.

doi: 10.1089/ten.teb.2009.0825

98. Im GI. Bone marrow-derived stem/stromal cells and adipose tissue-derived stem/stromal cells: Their comparative efficacies and synergistic effects. *J Biomed Mater Res Part A*. 2017;105(9):2640-2648.

doi: 10.1002/jbm.a.36089

99. Trzyna A, Banaś-Ząbczyk A. Adipose-derived stem cells secretome and its potential application in "stem cell-free therapy". *Biomolecules*. 2021;11(6):878.

doi: 10.3390/biom11060878

100. Chan YW, So C, Yau KL, *et al*. Adipose-derived stem cells and cancer cells fuse to generate cancer stem cell-like cells with increased tumorigenicity. *J Cell Physiol*. 2020;235(10):6794-6807.

doi: 10.1002/jcp.29574

101. Zhang J, Liu Y, Chen Y, *et al*. Adipose-derived stem cells: current applications and future directions in the regeneration of multiple tissues. *Stem Cells Int*. 2020;2020(1):8810813.

doi: 10.1155/2020/8810813

102. Choudhery MS, Badowski M, Muise A, *et al*. Donor age negatively impacts adipose tissue-derived mesenchymal stem cell expansion and differentiation. *J Transl Med*. 2014;12(1):8.

doi: 10.1186/1479-5876-12-8

103. Zhang Y, Zhuang H, Ren X, *et al*. Therapeutic effects of different intervention forms of human umbilical cord mesenchymal stem cells in the treatment of osteoarthritis. *Front Cell Dev Biol*. 2023;11:1246504.

doi: 10.3389/fcell.2023.1246504

104. Chen X, Zheng J, Yin L, *et al*. Transplantation of three mesenchymal stem cells for knee osteoarthritis, which cell and type are more beneficial? A systematic review and network meta-analysis. *J Orthop Surg Res*. 2024;19(1):366.

doi: 10.1186/s13018-024-04846-1

105. Yang Z, Wang B, Liu W, *et al*. In situ self-assembled organoid for osteochondral tissue regeneration with dual functional units. *Bioact Mater*. 2023;27:200-215.

doi: 10.1016/j.bioactmat.2023.04.002

106. Vaskovich-Koubi D, Buzhor MG, Krinsky A, *et al*. Patient-Derived 3D-Bioprinted models of pancreatic Cancer: Toward personalized therapy and overcoming tumor microenvironment challenges. *Adv Drug Delivery Rev*. 2025:115670.

doi: 10.1016/j.addr.2025.115670

107. Piotrowska U, Tsoi J, Singh P, *et al*. 3D bioprinting and artificial intelligence for tumor microenvironment modeling: a scoping review of models, methods, and integration pathways. *Mol Pharm*. 2025;22(10):5801-5823.

doi: 10.1021/acs.molpharmaceut.5c01062

108. Maggiotto F, Bova L, Micheli S, *et al*. 3D bioprinting for the production of a perfusable vascularized model of a cancer niche. *Front Bioeng Biotechnol*. 2025;13:1484738.

doi: 10.3389/fbioe.2025.1484738

109. Shukla AK, Shukla S, Suryawanshi SP, *et al*. High-throughput 3D bioprinted organoids of skin cancer utilized for diagnosis and personalized therapy. *Curr Oncol*. 2025;32(12):653.

doi: 10.3390/curroncol32120653

110. Souralova T, Rehakova D, Jeseta M, *et al*. The manufacture of xeno-and feeder-free clinical-grade human embryonic stem cell lines: First step for cell therapy. *Int J Mol Sci*.

2022;23(20):12500.

doi: 10.3390/ijms232012500

111. Esfahani SN, Irizarry AMR, Xue X, *et al*. Micro/nanoengineered technologies for human pluripotent stem cells maintenance and differentiation. *Nano Today*. 2021;41:101310.

doi: 10.1016/j.nantod.2021.101310

112. Posfai E, Lanner F, Mulas C, Leitch HG. All models are wrong, but some are useful: Establishing standards for stem cell-based embryo models. *Stem Cell Rep*. 2021;16(5):1117-1141.

doi: 10.1016/j.stemcr.2021.03.019

113. Fowler JL, Ang LT, Loh KM. A critical look: Challenges in differentiating human pluripotent stem cells into desired cell types and organoids. *Wiley Interdiscip Rev Dev Biol*. 2020;9(3):e368.

doi: 10.1002/wdev.368

114. Frederiksen HR, Glantz A, Vøls KK, *et al*. CRISPR-Cas9 immune-evasive hESCs are rejected following transplantation into immunocompetent mice. *Front Genome Ed*. 2024;6:1403395.

doi: 10.3389/fgeed.2024.1403395

115. Kim B, Kim J, Lee S. Unleashing the power of undifferentiated induced pluripotent stem cell bioprinting: current progress and future prospects. *Int J Stem Cells*. 2024;17(1):38-50.

doi: 10.15283/ijsc23146

116. Fu B, Shen J, Chen Y, *et al*. Narrative review of gene modification: applications in three-dimensional (3D) bioprinting. *Ann Transl Med*. 2021;9(19):1502.

doi: 10.21037/atm-21-2854

117. Dhaiban S, Chandran S, Noshi M, Sajini AA. Clinical translation of human iPSC technologies: advances, safety concerns, and future directions. *Front Cell Dev Biol*. 2025;13:1627149.

doi: 10.3389/fcell.2025.1627149

118. Cerneckis J, Cai H, Shi Y. Induced pluripotent stem cells (iPSCs): molecular mechanisms of induction and applications. *Signal Transduct Target Ther*. 2024;9(1):112.

doi: 10.1038/s41392-024-01809-0

119. Kim J-H, Kawase E, Bharti K, *et al*. Perspectives on the cost of goods for hPSC banks for manufacture of cell therapies. *npj Regener Med*. 2022;7(1):54.

doi: 10.1038/s41536-022-00242-7

120. Sawamoto N, Doi D, Nakanishi E, *et al*. Phase I/II trial of iPS-cell-derived dopaminergic cells for Parkinson's disease. *Nature*. 2025;641(8064):971-977.

doi: 10.1038/s41586-025-08700-0

121. Chen X, Ye S, Ying Q. Stem cell maintenance by manipulating signaling pathways: past, current and future. *BMB Rep*. 2015;48(12):668.

doi: 10.5483/BMBRep.2015.48.12.215

122. Liu TM, Tew W, Yang Z, *et al*. Understanding the molecular basis of mesenchymal stem cell stemness: implications for clinical applications. *Cell Death Dis*. 2025;16(1):778.

doi: 10.1038/s41419-025-08094-x

123. Afonso MB, Marques V, Van Mil SWC, Rodrigues CMP. Human liver organoids: From generation to applications. *Hepatology*. 2024;79(6):1432-1451.

doi: 10.1097/HEP.0000000000000343

124. Ma X, Qu X, Zhu W, *et al*. Deterministically patterned biomimetic human iPSC-derived hepatic model via rapid 3D bioprinting. *Proc Natl Acad Sci USA*. 2016;113(8):2206-2211.

doi: 10.1073/pnas.1524510113

125. Bhatia SN, Underhill GH, Zaret KS, Fox IJ. Cell and tissue engineering for liver disease. *Sci Transl Med*. 2014;6(245):245sr2.

doi: 10.1126/scitranslmed.3005975

126. Ali ASM, Wu D, Bannach-Brown A, *et al*. 3D bioprinting of liver models: A systematic scoping review of methods, bioinks, and reporting quality. *Mater Today Bio*. 2024;26:100991.

doi: 10.1016/j.mtbio.2024.100991

127. Shrestha S, Lekkala VKR, Acharya P, *et al*. Reproducible generation of human liver organoids (HLOs) on a pillar plate platform via microarray 3D bioprinting. *Lab Chip*. 2024;24(10):2747-2761.

doi: 10.1039/D4LC00149D

128. Yan J, Ye Z, Lu Y, *et al*. 3D bioprinting lobule-like hepatorganoids with induced vascularization for orthotopic implantation. *Mater Today Bio*. 2025;31:101515.

doi: 10.1016/j.mtbio.2025.101515

129. Yang H, Sun L, Pang Y, *et al*. Three-dimensional bioprinted hepatorganoids prolong survival of mice with liver failure. *Gut*. 2021;70(3):567-574.

doi: 10.1136/gutjnl-2019-319960

130. Xiang T, Wang J, Li H. Current applications of intestinal organoids: a review. *Stem Cell Res Ther*. 2024;15(1):155.

doi: 10.1186/s13287-024-03768-3

131. Sato T, Vries RG, Snippert HJ, *et al*. Single Lgr5 stem cells build crypt-villus structures in vitro without a mesenchymal niche. *Nature*. 2009;459(7244):262-265.

doi: 10.1038/nature07935

132. Pimenta J, Ribeiro R, Almeida R, *et al*. Organ-on-chip

approaches for intestinal 3D in vitro modeling. *Cell Mol Gastroenterol Hepatol*. 2022;13(2):351-367.

doi: 10.1016/j.jcmgh.2021.08.015

133. Kjar A, McFarland B, Mecham K, *et al*. Engineering of tissue constructs using coaxial bioprinting. *Bioact Mater*. 2021;6(2):460-471.

doi: 10.1016/j.bioactmat.2020.08.020

134. Li Y, Cheng S, Shi H, *et al*. 3D embedded bioprinting of large-scale intestine with complex structural organization and blood capillaries. *Biofabrication*. 2024;16(4):045001.

doi: 10.1088/1758-5090/ad5b1b

135. Torras N, Zabalo J, Abril E, *et al*. A bioprinted 3D gut model with crypt-villus structures to mimic the intestinal epithelial-stromal microenvironment. *Biomater Adv*. 2023;153:213534.

doi: 10.1016/j.bioadv.2023.213534

136. Finkbeiner SR, Freeman JJ, Wieck MM, *et al*. Generation of tissue-engineered small intestine using embryonic stem cell-derived human intestinal organoids. *Biol Open*. 2015;4(11):1462-1472.

doi: 10.1242/bio.013235

137. Jacob G, Shimomura K, Nakamura N. Osteochondral injury, management and tissue engineering approaches. *Front Cell Dev Biol*. 2020;8:580868.

doi: 10.3389/fcell.2020.580868

138. Faeed M, Ghiasvand M, Fareghzadeh B, Taghiyar L. Osteochondral organoids: current advances, applications, and upcoming challenges. *Stem Cell Res Ther*. 2024;15(1):183.

doi: 10.1186/s13287-024-03790-5

139. Doyle SE, Snow F, Duchi S, *et al*. 3D printed multiphasic scaffolds for osteochondral repair: challenges and opportunities. *Int J Mol Sci*. 2021;22(22):12420.

doi: 10.3390/ijms222212420

140. Cao B, Zhang K, Zuo R, *et al*. 3D-bioprinted functional scaffold based on synergistic induction of i-PRF and laponite exerts efficient and personalized bone regeneration via miRNA-mediated TGF-β/Smads signaling. *Int J Surg*. 2025;111(5):3193-3211.

doi: 10.1097/JS9.0000000000002312

141. Karam AS, Kronemberger GS, Chattahy K, Kelly DJ. Cell-only bioprinting of articular cartilage progenitor cells within a physically constraining support bath to engineer structurally organized grafts. *Bioact Mater*. 2026;59:251-265.

doi: 10.1016/j.bioactmat.2025.12.013

142. Jiao Y, Lu S, Zhang J, Zhen J. Applications in osteochondral organoids for osteoarthritis research: from pathomimetic modeling to tissue engineering repair. *Front Bioeng Biotechnol*. 2025;13:1629608.

doi: 10.3389/fbioe.2025.1629608

143. Chen Z, Bo Q, Wang C, *et al*. Single BMSC-derived cartilage organoids for gradient heterogeneous osteochondral regeneration by leveraging native vascular microenvironment. *J Nanobiotechnol*. 2025;23(1):325.

doi: 10.1186/s12951-025-03403-0

144. Bowes A, Collins A, Oakley F, *et al*. Bioprinted high-cell-density laminar scaffolds stimulate extracellular matrix production in osteochondral co-cultures. *Int J Mol Sci*. 2024;25(20):11131.

doi: 10.3390/ijms252011131

145. Xiao Y, Li Y, Jing X, *et al*. Organoid models in oncology: advancing precision cancer therapy and vaccine development. *Cancer Biol Med*. 2025;22(8):903-927.

doi: 10.20892/j.issn.2095-3941.2025.0127

146. Wang X, Luo Y, Ma Y, *et al*. Converging bioprinting and organoids to better recapitulate the tumor microenvironment. *Trends Biotechnol*. 2024;42(5):648-663.

doi: 10.1016/j.tibtech.2023.11.006

147. Mao S, Xie R, Shou J, *et al*. Bioprinting of patient-derived heterogeneous renal cell carcinoma organoids for personalized therapy. *Biofabrication*. 2025;17(4):045008.

doi: 10.1088/1758-5090/adecc5

148. Zhang F, Lin DSY, Rajasekar S, *et al*. Pump-less platform enables long-term recirculating perfusion of 3D printed tubular tissues. *Adv Healthcare Mater*. 2023;12(27):e2300423.

doi: 10.1002/adhm.202300423

149. Formica C, Addario G, Fagiolino S, *et al*. Microfluidic bioprinting as a tool to produce hiPSCs-derived renal organoids. *Biofabrication*. 2025;17(3):035016.

doi: 10.1088/1758-5090/addb7e

150. Shin J, Tabatabaei Rezaei N, Choi S, *et al*. Photocrosslinkable kidney decellularized extracellular matrix-based bioink for 3D bioprinting. *Adv Healthcare Mater*. 2025;14(24):e2501616.

doi: 10.1002/adhm.202501616

151. Fransen MFJ, Addario G, Bouten CVC, *et al*. Bioprinting of kidney in vitro models: cells, biomaterials, and manufacturing techniques. *Essays Biochem*. 2021;65(3):587-602.

doi: 10.1042/ebc20200158

152. Yang H, Zhang J, Li Y, *et al*. Multiscale organization of neural networks in a 3D bioprinted matrix. *Adv Sci*. 2025;12(30):e04455.

doi: 10.1002/advs.202504455

153. Choi T, Park J, Lee S, *et al*. 3D bioprinted neural tissues: emerging strategies for regeneration and disease modeling.

Pharmaceutics. 2025;17(9):1176.

doi: 10.3390/pharmaceutics17091176

154. Kupfer ME, Lin WH, Ravikumar V, *et al*. In situ expansion, differentiation, and electromechanical coupling of human cardiac muscle in a 3D bioprinted, chambered organoid. *Circ Res*. 2020;127(2):207-224.

doi: 10.1161/circresaha.119.316155

155. Fang Y, Guo Y, Wu B, *et al*. Expanding embedded 3D bioprinting capability for engineering complex organs with freeform vascular networks. *Adv Mater*. 2023;35(22):e2205082.

doi: 10.1002/adma.202205082

156. Kim MS, Choi Y, Lee KY. Three-dimensional printing and bioprinting strategies for cardiovascular constructs: from printing inks to vascularization. *Polymers*. 2025;17(17)

doi: 10.3390/polym17172337

157. Wang Y, Liu A, Lin Y, *et al*. A rational framework for 3D bioprinting of organoids: From assembly mechanisms and material properties to functional outcomes. *Int J Bioprint*. 2026;12(2):2337.

doi: 10.36922/ijb025010539

158. Lv W, Zhou H, Aazmi A, *et al*. Constructing biomimetic liver models through biomaterials and vasculature engineering. *Regen Biomater*. 2022;9:rbac079.

doi: 10.1093/rb/rbac079

159. Saiki N, Nio Y, Yoneyama Y, *et al*. Self-organization of sinusoidal vessels in pluripotent stem cell-derived human liver bud organoids. *Nat Biomed Eng*. 2025;9(11):1869-1885.

doi: 10.1038/s41551-025-01416-6

160. Brassard JA, Nikolaev M, Hübscher T, *et al*. Recapitulating macro-scale tissue self-organization through organoid bioprinting. *Nat Mater*. 2021;20(1):22-29.

doi: 10.1038/s41563-020-00803-5

161. Rea M, Lisa LD, Pagnotta G, *et al*. Establishing a bioink assessment protocol: GelMA and collagen in the bioprinting of a potential in vitro intestinal model. *ACS Biomater Sci Eng*. 2025;11(4):2456-2467.

doi: 10.1021/acsbiomaterials.5c00034

162. Gao Z, Du H, Yu S, *et al*. 3D bioprinted human-scale intestine models for physiological and microbial insights through fluid-driven heterogeneity. *Sci Adv*. 2025;11(47):eady6562.

doi: 10.1126/sciadv.ady6562

163. Ren J, Huang S. Intestinal organoids in inflammatory bowel disease: advances, applications, and future directions. *Front Cell Dev Biol*. 2025;13:1517121.

doi: 10.3389/fcell.2025.1517121

164. Truong H, Guvendiren M. Bioprinting the osteochondral interface: advances, challenges, and future directions. *Tissue Eng Part A*. Published online January 7, 2025

doi: 10.1177/19373341251410101

165. Jahangir S, Vecstaudza J, Augurio A, *et al*. Cell-laden 3D printed GelMA/HAp and THA hydrogel bioinks: development of osteochondral tissue-like bioinks. *Materials*. 2023;16(22):7214.

doi: 10.3390/ma16227214

166. Nedrelow DS, Townsend JM, Detamore MS. Osteochondral regeneration with anatomical scaffold 3D-printing-design considerations for interface integration. *J Biomed Mater Res Part A*. 2025;113(1):e37804.

doi: 10.1002/jbm.a.37804

167. Cui X, Jiao J, Yang L, *et al*. Advanced tumor organoid bioprinting strategy for oncology research. *Mater Today Bio*. 2024;28:101198.

doi: 10.1016/j.mtbio.2024.101198

168. Spagnol G, Sensi F, De Tommasi O, *et al*. Patient derived organoids (PDOs), extracellular matrix (ECM), tumor microenvironment (TME) and drug screening: state of the art and clinical implications of ovarian cancer organoids in the era of precision medicine. *Cancers*. 2023;15(7):2059.

doi: 10.3390/cancers15072059

169. Zhang C, Wang Q, Li K, *et al*. Mechanoadaptation via myosin cytoplasmic redistribution protects circulating tumor cells from shear-induced death during hematogenous dissemination. *Adv Sci*. 2026;13(33):e23112.

doi: 10.1002/advs.202523112

170. Lawlor KT, Vanslambrouck JM, Higgins JW, *et al*. Cellular extrusion bioprinting improves kidney organoid reproducibility and conformation. *Nat Mater*. 2021;20(2):260-271.

doi: 10.1038/s41563-020-00853-9

171. Homan KA, Gupta N, Kroll KT, *et al*. Flow-enhanced vascularization and maturation of kidney organoids in vitro. *Nat Methods*. 2019;16(3):255-262.

doi: 10.1038/s41592-019-0325-y

172. Tabibzadeh N, Satlin LM, Jain S, Morizane R. Navigating the kidney organoid: insights into assessment and enhancement of nephron function. *Am J Physiol Renal Physiol*. 2023;325(6):F695-F706.

doi: 10.1152/ajprenal.00166.2023

173. Layrolle P, Payoux P, Chavanas S. Message in a scaffold: natural biomaterials for three-dimensional (3D) bioprinting of human brain organoids. *Biomolecules*. 2023;13(1):25.

doi: 10.3390/biom13010025

174. Tan S, Qiu L, Lee JWL, Zeng L. Advances in 3D bioprinting for modeling the blood-brain barrier in neurodegenerative

diseases. *Front Mol Biosci*. 2025;12:1703403.

doi: 10.3389/fmolb.2025.1703403

175. Yin J, Yan M, Wang Y, *et al*. 3D bioprinting of low-concentration cell-laden gelatin methacrylate (GelMA) bioinks with a two-step cross-linking strategy. *ACS Appl Mater Interfaces*. 2018;10(8):6849-6857.

doi: 10.1021/acsami.7b16059

176. Wolfe JT, He W, Kim MS, *et al*. 3D-bioprinting of patient-derived cardiac tissue models for studying congenital heart disease. *Front Cardiovasc Med*. 2023;10:1162731.

doi: 10.3389/fcvm.2023.1162731

177. Leung MC, Laksman Z. 3D bioprinting functional engineered heart tissues. *Int J Mol Sci*. 2025;26(21):10707.

doi: 10.3390/ijms262110707

178. Roche CD, Brereton RJL, Ashton AW, *et al*. Current challenges in three-dimensional bioprinting heart tissues for cardiac surgery. *Eur J Cardiothorac Surg*. 2020;58(3):500-510.

doi: 10.1093/ejcts/ezaa093

179. Kato B, Wisser G, Agrawal DK, *et al*. 3D bioprinting of cardiac tissue: current challenges and perspectives. *J Mater Sci Mater Med*. 2021;32(5):54.

doi: 10.1007/s10856-021-06520-y

180. Shapira A, Dvir T. 3D tissue and organ printing—hope and reality. *Adv Sci*. 2021;8(10):2003751.

doi: 10.1002/advs.202003751

181. Liu F, Quan R, Vyas C, Aslan E. Hybrid biomanufacturing systems applied in tissue regeneration. *Int J Bioprint*. 2022;9(1):646.

doi: 10.18063/ijb.v9i1.646

182. Bercea M. Rheology as a tool for fine-tuning the properties of printable bioinspired gels. *Molecules*. 2023;28(6):2766.

doi: 10.3390/molecules28062766

183. Bertassoni LE. Bioprinting of complex multicellular organs with advanced functionality—recent progress and challenges ahead. *Adv Mater*. 2022;34(3):2101321.

doi: 10.1002/adma.202101321

184. Teixeira MC, Lameirinhas NS, Carvalho JPF, *et al*. A guide to polysaccharide-based hydrogel bioinks for 3D bioprinting applications. *Int J Mol Sci*. 2022;23(12):6564.

doi: 10.3390/ijms23126564

185. Zhang S, Xu G, Wu J, *et al*. Microphysiological constructs and systems: biofabrication tactics, biomimetic evaluation approaches, and biomedical applications. *Small Methods*. 2024;8(1):2300685.

doi: 10.1002/smtd.202300685

186. Seymour AJ, Westerfield AD, Cornelius VC, *et al*. Bioprinted microvasculature: progressing from structure to function. *Biofabrication*. 2022;14(2):022002.

doi: 10.1088/1758-5090/ac4fb5

187. Al Qassab M, Merheb M, Sayadi S, *et al*. Organ-specific strategies in bioprinting: Addressing translational challenges in the heart, liver, kidney, and pancreas. *J Funct Biomater*. 2025;16(10):356.

doi: 10.3390/jfb16100356

188. Malkani S, Prado O, Stevens KR. Sacrificial templating for accelerating clinical translation of engineered organs. *ACS Biomater Sci Eng*. 2024;11(1):1-12.

doi: 10.1021/acsbiomaterials.4c01824

189. Wang K, Lan X, Chen J, *et al*. One-step coaxial 3D printing of pre-vascularized skin organoid models with ADSC microspheres for enhanced wound healing. *Adv Sci*. 2026;13(9):e17409.

doi: 10.1002/advs.202517409

190. Zhao X, Xu Z, Xiao L, *et al*. Review on the vascularization of organoids and organoids-on-a-Chip. *Front Bioeng Biotechnol*. 2021;9:637048.

doi: 10.3389/fbioe.2021.637048

191. Urbischek M, Rannikmae H, Foets T, *et al*. Organoid culture media formulated with growth factors of defined cellular activity. *Sci Rep*. 2019;9(1):6193.

doi: 10.1038/s41598-019-42604-0

192. Tashman JW, Shiwarski DJ, Feinberg AW. Development of a high-performance open-source 3D bioprinter. *Sci Rep*. 2022;12(1):22652.

doi: 10.1038/s41598-022-26809-4

193. Lee H. Engineering in vitro models: Bioprinting of organoids with artificial intelligence. *Cyborg Bionic Syst*. 2023;4:0018.

doi: 10.34133/cbsystems.0018

194. Xie Z, Wang L, Zhang Y. Advances in organoid culture research. *Glob Med Genet*. 2022;09(04):268-276.

doi: 10.1055/s-0042-1756662

195. Gomes Gama JF, Dias EA, Aguiar Coelho RMG, *et al*. Development and implementation of a significantly low-cost 3D bioprinter using recycled scrap material. *Front Bioeng Biotechnol*. 2023;11:1108396.

doi: 10.3389/fbioe.2023.1108396

196. Atala A, Bischof JC, Chen CS, *et al*. The need for an organoid manufacturing, preservation, and distribution center. *Stem Cells Transl Med*. 2025;14(7):szaf031.

doi: 10.1093/stcltm/szaf031

197. Wang X, Zhang D, Singh YP, *et al*. Progress in organ bioprinting for regenerative medicine. *Engineering*.

2024;42:121-142.

doi: 10.1016/j.eng.2024.04.023

198. Davoodi E, Li J, Ma X, *et al*. Imaging-guided deep tissue in vivo sound printing. *Science*. 2025;388(6747):616-623.

doi: 10.1126/science.adt0293

199. Li Z, Chen L, Wu J, *et al*. A review of 3D bioprinting for organoids. *Med Rev*. 2025;5(4):318-338.

doi: 10.1515/mr-2024-0089

200. Roy N, Cucullo L. Organs-on-chips in drug development: engineering foundations, artificial intelligence, and clinical translation. *Biosensors*. 2026;16(3):155.

doi: 10.3390/bios16030155

201. Zhang Y, Wang F, Li R, *et al*. Immune-instructive bone organoids via non-immunogenic plant-based bioinks for enhanced bone repair. *Matter*. 2026;9(4):102651.

doi: 10.1016/j.matt.2026.102651

202. Yeh Y, Chen P, Chen K, Lee IC. Innovative MXene/SilMA-based conductive bioink for three dimensional bioprinting of neural stem cell spheroids in neural tissue engineering. *ACS Appl Mater Interfaces*. 2025;17(7):10402-10416.

doi: 10.1021/acsami.4c19373

203. Marques DMC, Jabouille M, Gusmão A, *et al*. Microalgae-enriched (bio) inks for 3D bioprinting of cultured seafood. *npj Sci Food*. 2025;9(1):23.

doi: 10.1038/s41538-025-00386-y

204. Deng B, Lasaosa FL, Chen D, *et al*. An interactive Bayesian optimization framework for intelligent design of HAMA/GelMA hybrid hydrogels. *Polym Test*. 2026;156:109132.

doi: 10.1016/j.polymertesting.2026.109132

205. Shin J, Kang R, Hyun K, *et al*. Machine learning-enhanced optimization for high-throughput precision in cellular droplet bioprinting. *Adv Sci*. 2025;12(20):e2412831.

doi: 10.1002/advs.202412831

206. Chen Y, Yang X, Zhang Y, *et al*. Flowerbed-inspired biomimetic 3D-printed scaffolds functionalized with urine-derived stem cell exosomes promote alveolar bone regeneration by regulating energy metabolism. *Theranostics*. 2026;16(7):3826-3856.

doi: 10.7150/thno.123700

207. Filippi M, Mekkattu M, Katzschmann RK. Sustainable biofabrication: from bioprinting to AI-driven predictive methods. *Trends Biotechnol*. 2025;43(2):290-303.

doi: 10.1016/j.tibtech.2024.07.002

208. Bai L, Su J. Artificial intelligence virtual organoids (AIVOs). *Bioact Mater*. 2026;59:45-68.

doi: 10.1016/j.bioactmat.2025.12.030

209. Balkhair O, Albalushi H. Artificial intelligence in organoid-based disease modeling: a new frontier in precision medicine. *Biomimetics*. 2025;10(12):845.

doi: 10.3390/biomimetics10120845

210. Silva Robazzi JV, Derman ID, Gupta D, *et al*. The synergy of artificial intelligence and 3D bioprinting: unlocking new frontiers in precision and tissue fabrication. *Adv Funct Mater*. 2025;36(1).

doi: 10.1002/adfm.202509530

211. Huang D, Li Z, Li G, *et al*. Biomimetic structural design in 3D-printed scaffolds for bone tissue engineering. *Mater Today Bio*. 2025;32:101664.

doi: 10.1016/j.mtbio.2025.101664

212. Zhang Z, Zhou X, Fang Y, *et al*. AI-driven 3D bioprinting for regenerative medicine: From bench to bedside. *Bioact Mater*. 2025;45:201-230.

doi: 10.1016/j.bioactmat.2024.11.021